Critical Behavior of a Compressible Ising Ferromagnet Examined by Monte Carlo Simulations

Master-Thesis von Dominic Spiller
Tag der Einreichung:

1. Gutachten: Apl. Prof. Dr. Burkhard Dünweg
2. Gutachten: Dr. Andreas Tröster

TECHNISCHE
UNIVERSITÄT
DARMSTADT

Fachbereich Physik
Institut für Festkörperphysik

Critical Behavior of a Compressible Ising Ferromagnet Examined by Monte Carlo Simulations

Vorgelegte Master-Thesis von Dominic Spiller

1. Gutachten: Apl. Prof. Dr. Burkhard Dünweg
2. Gutachten: Dr. Andreas Tröster

Tag der Einreichung:

Erklärung zur Master-Thesis

Hiermit versichere ich, die vorliegende Master-Thesis ohne Hilfe Dritter nur mit den angegebenen Quellen und Hilfsmitteln angefertigt zu haben. Alle Stellen, die aus Quellen entnommen wurden, sind als solche kenntlich gemacht. Diese Arbeit hat in gleicher oder ähnlicher Form noch keiner Prüfungsbehörde vorgelegen.

Darmstadt, den 15.09.16

(Dominic Spiller)

Abstract

The critical behavior of an Ising model coupled to elastic degrees of freedom is examined. If linear elasticity theory is assumed, the latter can be eliminated in the theoretic model. The theory then predicts a second order phase transition with Fisher renormalized exponents in the constant volume case. The model used in simulation however, includes all elastic interactions. Evaluation shows, that in the present case there is no evidence for Fisher renormalization. Instead, within precision the standard Ising values of the critical exponents are found.

An alternative set of parameters is proposed in order to increase the effect of elastic coupling. In a first step the ground state is examined with the second set of parameters. It is found, that additional to the magnetic phase transition, there is a structural transition from a clustered to an unclustered state.

Acknowledgments

Firstly, I would like to thank Prof. Dünweg for his support throughout this thesis. He never hesitated to spend large amounts of his time for enlightening discussions on the topic. I was able to work freely on the topic, but was always steered in the right direction if necessary.

Also I would like to express my gratitude to AG Drossel for giving me access to their computational resources, as well as the administration team for always promptly solving any problem.

Last but not least, I must thank my parents for unconditionally supporting me throughout my studies. This would not have been possible without them.

Contents

1 Introduction

Since the Ising model was invented in 1920 it has been subject to ongoing research. Applications of the Ising model include not only the modeling of magnets, but also binary alloys [1] lattice gases, spin glasses and even the modeling of neurons [2]. From a physicists' point of view, it seems only natural to consider the addition of elastic degrees of freedom, since real bodies are always to some extent elastic.

In the present work, Monte Carlo simulations of a microscopic model are conducted in order to examine the influence of the elastic coupling on the critical behavior. In comparison to experiment, simulations offer the advantage, that a very strong coupling can be chosen, which should result in a more distinct effect of the elastic degrees of freedom.

There already exists some theoretical research on this topic. It was argued, that for constant volume there should be a second order phase transition with Fisher renormalized critical exponents [3, 4, 5, 6, 7, 8], where the renormalized exponents are actually in better agreement with experimental values, than the regular Ising exponents [3]. In the references cited above, a linear theory of elasticity was assumed. This allows for the elimination of the microscopic elastic degrees from the effective Hamiltonian.

That an effective Hamiltonian of this kind does indeed produce Fisher renormalized exponents has been confirmed by simulation by A. Tröster [9]. The model simulated in the present work, however, does include all elastic degrees of freedom. The objective is, to test the validity of the assumptions made in theory, by using a model, that still includes all the interactions.

The structure of the present thesis is as follows: In Chapter 2, a review of the field theory of the regular Ising model is given. This is used as basis to derive an effective Hamiltonian by adding terms of the elastic energy and coupling. Also the methods, that are later used to evaluate the data, are discussed. This includes finite-size scaling, the multi histogram reweighting method and the blocking method for calculating error values from correlated data. It is shown, that the Swendsen-Wang cluster algorithm is indeed a valid simulation method for the present model. Finally, The microscopic model as it is simulated in this work is introduced and the details of implementation are discussed.

In Chapter 3, a finite-size scaling analysis is conducted to determine the critical exponents of the system. An alternative parameter set is proposed and the structural properties of the ground state are examined for said parameters. Also, the magnetic properties for $T > 0$ are reviewed. It follows a summary and an outlook for the future work that can be done on this topic.

2 Theory

In this chapter, the theoretical basis of this work is given. We will start by giving a brief repetition of the standard Ising model without any elastic degrees of freedom. The Landau-Ginzburg-Wilson (LGW) Hamiltonian is motivated to provide a field theoretical description of the Ising model on the basis of the order parameter.

The transition to the compressible Ising model is done by adding expressions for the elastic energy and the coupling energy to the LGW Hamiltonian. The critical behavior of the effective Hamiltonian is then discussed for constant pressure and constant volume.

In the next section, the methods of finite-size scaling are outlined. Several relations are derived, which are used to determine the critical exponents of the compressible Ising model later on.

The multi histogram reweighting method is described in the following section. It is a powerful tool, that can be used to combine the statistical data from multiple simulations and reweight observables to temperatures, where no actual simulations have been done.

Next, the blocking method for error calculations is discussed. Since Monte Carlo simulations are Markov chains, the individual data points are intercorrelated and we cannot use simple Gaussian statistics to compute the errors. With the blocking method the data set is reduced to a stage, where only uncorrelated points remain. These can in turn be used, to compute the correct error by ordinary Gaussian statistics.

2.1 The "Rigid" Ising Model

The Ising model is one of the most established models to describe a phase transition. Magnetic dipole moments are represented by spins S_i on a lattice as illustrated in Fig. 2.1. The spins can take exactly two states, namely $S_i = \pm 1$ and are coupled to their nearest neighbors by a coupling constant J. The Hamiltonian of the Ising model is

$$\mathcal{H}_{\text{Ising}} = -J \sum_{\langle ij \rangle} S_i S_j - H \sum_i S_i, \tag{2.1}$$

where H is an optional external magnetic field, which couples to all the spins. Angular brackets indicate, that only pairs i, j of nearest neighbors are taken into account in the sum. If the coupling constant J is positive, the system is ferromagnetic. As a consequence parallel spins will reduce the total energy. In the absence of an external field, i.e. $H = 0$, the Hamiltonian is symmetric under spin inversion $S_i \to -S_i$. The order parameter of the Ising model is the magnetization m:

$$m = \frac{1}{N} \sum_{i=1}^{N} S_i, \tag{2.2}$$

where N is the number of spins in the system. In the ordered state, which has lower symmetry, the majority of spins will have the same state and therefore $m \neq 0$. In the disordered state, being the state with higher symmetry, the value of the spins is random and $m = 0$. The order parameter is therefore a measure of the deviation from the symmetrical state. However, this only holds in the thermodynamic limit (i.e. systems of infinite size). In finite systems, there is no phase transition in the strict sense. In this case, the system jumps between two equivalent magnetizations $\pm m_{\text{sp}}$ effectively yielding $\langle m \rangle = 0$. For an example see Fig. 2.2. For the Metropolis algorithm this becomes less likely with increasing system size, as the statistical weight of the connecting states decreases. This problem can however be circumvented by the Swendsen-Wang algorithm, which flips clusters of spins rather than individual spins (See Sec. 2.6). Despite the fact, that $\langle m \rangle = 0$ in finite systems, we can differentiate between ordered and disordered systems by simply sampling the symmetrized order parameter $|m|$.

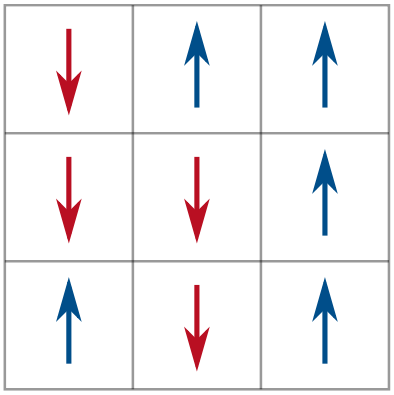

Figure 2.1: Illustration of the $d = 2$ Ising model as spins on a lattice

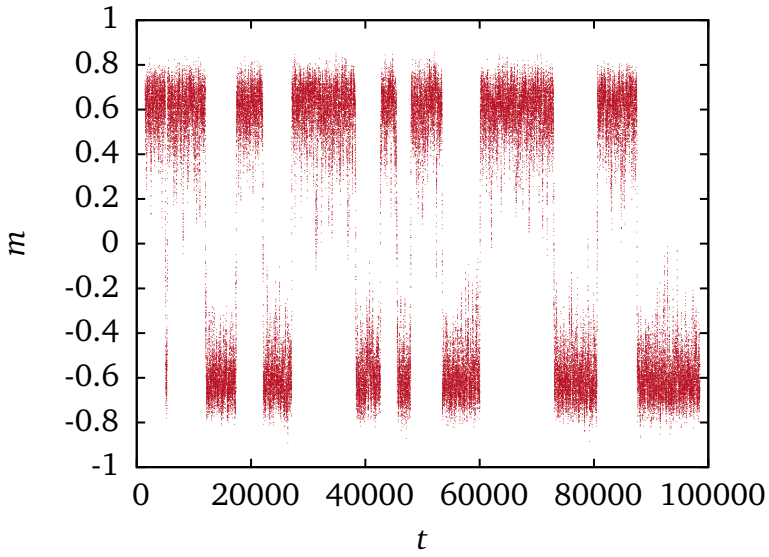

Figure 2.2: Time series of the magnetization m computed with the Metropolis Algorithm with $\kappa = 1$, $K = 3$, $L = 10$ and $T = 6.7 < T_c$. Throughout the time series, the system stays at one magnetization m_{sp} for several thousand steps before switching to the equivalent magnetization $-m_{sp}$. For short runs, this leads to an asymmetric distribution $P(m)$.

In $d = 3$, the temperature driven phase transition of the Ising model is of *second order*. When the temperature is increased starting at $T = 0$, the order parameter will drop continuously, until it becomes zero at the critical temperature T_c. This is contrary to first order phase transitions, where the order parameter has a discontinuous jump at T_c. For second order phase transitions however, the decrease of the order parameter near T_c is well described by a power law. In the Ising model we can write

$$|m| \propto |T - T_c|^{\beta} \tag{2.3}$$

for $T \lesssim T_c$. In a system of finite-size, the correlation length cannot diverge. As a consequence, the curve flattens out near T_c. This is illustrated in Fig. 2.3 (also see 2.9), where data from the simulation of a finite system is compared with the theory of infinite systems. Correlation length ξ, susceptibility χ and heat capacity C diverge at the critical temperature with the power laws

$$\xi \propto |T - T_c|^{-\nu}, \tag{2.4}$$
$$\chi \propto |T - T_c|^{-\gamma}, \tag{2.5}$$
$$C \propto |T - T_c|^{-\alpha}. \tag{2.6}$$

In finite systems, these divergences become peaks of bounded height.

The theory of finite-size scaling makes use of the fact, that those deviations from the ideal case obey strict laws themselves. This enables us to obtain very exact estimates of the critical temperature and exponents, even though only relatively small systems are simulated. For a derivation of the power laws above, as well as finite-size scaling relations see Sec. 2.3.

In order to describe the dependence of the energy on the order parameter we will use the Landau-Ginzburg-Wilson (LGW) field theory. Here, the order parameter $\phi(\mathbf{r})$ is allowed to

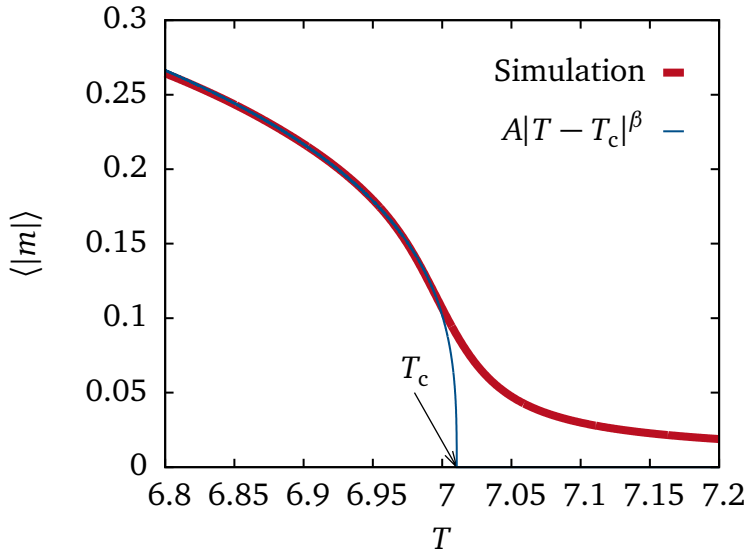

Figure 2.3: Behavior of the magnetization $|m|$ near the critical temperature T_c. The blue line is the power law given in Eq. (2.3). The red line is taken from simulation and illustrates the flattening of the curve due to finite size effects.

fluctuate in space ($\phi(\mathbf{r})$ is also called 'order parameter field'). The Hamiltonian of the LGW theory is given by the integral

$$\mathscr{H}_{\mathrm{LGW}} = \int \mathrm{d}^d\mathbf{r}\left(\frac{R}{2}(\boldsymbol{\nabla}\phi(\mathbf{r}))^2 + \frac{r_0}{2}\phi^2(\mathbf{r}) + \frac{u_0}{4!}\phi^4(\mathbf{r}) - H\phi(\mathbf{r})\right). \tag{2.7}$$

The first term is the interfacial energy with $R > 0$. In those points, where two regions with different order parameter meet, the gradient of the order parameter is non-zero. Since the interfacial energy is independent of the direction of the gradient, the second order term is the first relevant term in Taylor expansion.

The next two terms correspond to a power series expansion of the free energy up to the fourth order. For the parameter of the second order term $r_0 \propto T - T_c^{\mathrm{MF}}$ holds, T_c^{MF} being the critical temperature in mean field approximation. For the parameter of the fourth order term we will (for now) assume, that only even powers are included in the power series expansion, in order to ensure spin inversion symmetry. The last term takes into account an external magnetic field H and adds a bias towards $\phi > 0$ or $\phi < 0$.

In order to give an intuition of the LGW-Hamiltonian, we set $H = 0$ and do the mean field approximation $\phi(\mathbf{r}) \to \phi$. This way we can evaluate the integral and receive

$$\mathscr{H}_{\mathrm{LGW}}^{\mathrm{MF}} = V\left(\frac{r_0}{2}\phi^2 + \frac{u_0}{4!}\phi^4\right), \tag{2.8}$$

which just corresponds to a Landau expansion of the free energy up to the fourth order [10, 11, 12]. The Landau free energy (2.8) is plotted in Fig. 2.4 for different temperatures. As the temperature approaches T_c^{MF} from high temperatures, the fourth order term becomes increasingly dominant and results in a broad minimum at $T = T_c$, allowing for strong fluctuations. Moving below T_c^{MF}, the second order term becomes negative and two minimums develop at the origin. They move apart continuously as temperature is decreased further, which is the typical

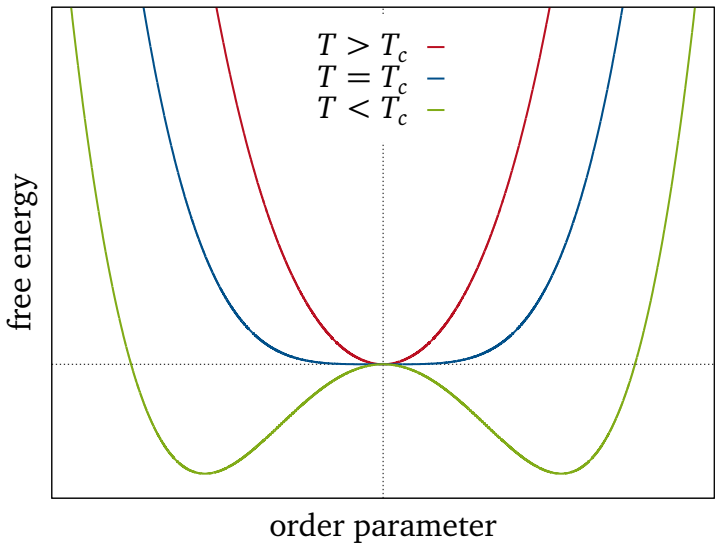

Figure 2.4: Landau free energy for different temperatures. The power series expansion was carried out up to the fourth order.

second order phase transition behavior. Since the order parameter minimizes the free energy in thermal equilibrium, these two minimums correspond to two equivalent ordered phases. In the Ising model, these are the spontaneous magnetizations $\pm m_{\mathrm{sp}}$.

2.2 The Compressible Ising Model

The compressible Ising model can be imagined as a standard Ising model on a elastic lattice. In the following, we will assume a lattice with cubic symmetry.

The interaction energy of the compressible Ising model is composed of three parts: The magnetic energy, the elastic energy and the coupling energy, resulting from the coupling between magnetic and elastic degrees of freedom. For the magnetic interaction, the Landau-Ginzburg-Wilson Hamiltonian from the standard Ising theory is used. A linear theory of elasticity is used, in order to derive an expression for the elastic energy. The expression for coupling is of the lowest order agreeing with the systems symmetries. From the sum of the three contributions an effective Hamiltonian is derived, which is then used to predict the critical behavior of the system.

2.2.1 Elastic Energy

The following derivations are largely taken from [4]. For the computation of the elastic energy, consider a d-dimensional isotropic solid with volume $V = L^d$. A small macroscopic deformation of the box can be described by the coordinate transformation

$$\mathbf{r}' = (\mathbf{1} + \mathbf{E})\tilde{\mathbf{r}}, \tag{2.9}$$

where $\tilde{\mathbf{r}}$ is the coordinate vector before deformation, $\mathbf{r}'$ is the coordinate vector after deformation and $\mathbf{1}$ is the unit matrix. Since a macroscopic rotation is not of interest, the *macroscopic strain tensor* $\mathbf{E}$ must be symmetric.

Additionally, we would like to consider small microscopic fluctuations, which we describe by the displacement $\mathbf{u}_0(\mathbf{r})$ of a volume element from its original position $\mathbf{r}$

$$\tilde{\mathbf{r}} = \mathbf{r} + \mathbf{u}_0(\mathbf{r}). \tag{2.10}$$

The total deflection $\mathbf{u}$ is then made up of both macroscopic deformation and microscopic fluctuation:

$$\begin{aligned} \mathbf{u}(\mathbf{r}) =& \mathbf{r}' - \mathbf{r} \\ =& \mathbf{u}_0(\mathbf{r}) + \mathbf{E}\mathbf{r} + \mathbf{E}\mathbf{u}_0(\mathbf{r}). \end{aligned} \tag{2.11}$$

Assuming, that $\mathbf{E}$ and $\mathbf{u}_0$ are small, this can be linearized to

$$\mathbf{u}(\mathbf{r}) = \mathbf{E}\mathbf{r} + \mathbf{u}_0(\mathbf{r}). \tag{2.12}$$

In the next step, we use the Fourier representation of the displacement field $\mathbf{u}_0$:

$$\mathbf{u}(\mathbf{r}) = \mathbf{E}\mathbf{r} + \sum_{\mathbf{k}\neq 0} \sum_{\lambda=0}^{d-1} \tilde{u}^{(\lambda)}(\mathbf{k}) \epsilon^{(\lambda)}(\mathbf{k}) \exp(\mathrm{i}\mathbf{k}\cdot\mathbf{r}). \tag{2.13}$$

The vector $\mathbf{k}$ is quantized like $\mathbf{k} = 2\pi\mathbf{n}/L$ with $\mathbf{n} \in \mathbb{Z}^d$. The value $\mathbf{k} = 0$ is omitted, since it merely represents a simple translation of the whole box. Different polarizations are represented

by the unit vectors $\boldsymbol{\epsilon}^{(\lambda)}$, where $\lambda = 0$ gives the longitudinal polarization $\boldsymbol{\epsilon}^{(0)} \parallel \mathbf{k}$, and $\lambda = 1, \ldots, d-1$ give the transversal polarizations $\boldsymbol{\epsilon}^{(i)} \perp \mathbf{k}$. These so called polarization vectors are orthonormalized, i.e. $\boldsymbol{\epsilon}^{(\lambda)} \cdot \boldsymbol{\epsilon}^{(\mu)} = \delta_{\lambda\mu}$. Additionally, for the displacement field $\mathbf{u}(\mathbf{r})$ to be real, the symmetry relations

$$\boldsymbol{\epsilon}^{(\lambda)}(-\mathbf{k}) = -\boldsymbol{\epsilon}^{(\lambda)}(\mathbf{k}), \tag{2.14}$$

$$\tilde{u}^{(\lambda)}(-\mathbf{k}) = -\left(\tilde{u}^{(\lambda)}(\mathbf{k})\right)^* \tag{2.15}$$

must be satisfied.

For the next step, we introduce the *microscopic strain tensor* $e_{\alpha\beta}$. Note, that in the following the Einstein summation convention is used, which implies the summation over all double Greek indexes in one term. For *small displacements*, the microscopic strain tensor is linked to the displacement as follows [13]:

$$e_{\alpha\beta} = \frac{1}{2}\left(\frac{\partial u_\alpha}{\partial r_\beta} + \frac{\partial u_\beta}{\partial r_\alpha}\right). \tag{2.16}$$

From the definition it is obvious, that the microscopic strain tensor is symmetric. Since for every tensor the trace is conserved under coordinate transformation, a natural way of representing a symmetric tensor, is to split it up into the sum of a multiple of the unit tensor and a traceless, symmetric tensor:

$$e_{\alpha\beta} = \frac{1}{d}\delta_{\alpha\beta}e_{\gamma\gamma} + \left(e_{\alpha\beta} - \frac{1}{d}\delta_{\alpha\beta}e_{\gamma\gamma}\right). \tag{2.17}$$

The first term in Eq. (2.17) represents a pure compression/dilation, whereas the second term represents a pure shear.

For the derivation of the elastic free energy density f in terms of the strain tensor $e_{\alpha\beta}$, we will assume *small deformations* and expand f into powers of $e_{\alpha\beta}$. In the undeformed state, the internal stresses in the body must be zero, i.e. $\sigma_{\alpha\beta} = 0$. The stress tensor $\sigma_{\alpha\beta}$ is defined as

$$\sigma_{\alpha\beta} = \frac{\partial f}{\partial u_{\alpha\beta}}. \tag{2.18}$$

This means, that there cannot be any linear terms in the expansion of f in powers of $e_{\alpha\beta}$. We can therefore assume a quadratic dependence of f, neglecting higher orders. Also the terms of f must be scalar, since f itself is scalar. Because $e_{\alpha\beta}$ is symmetric, it can be decomposed into two independent scalars of second order. These are the square of the trace $e_{\gamma\gamma}e_{\delta\delta}$ and the trace of the square $e_{\alpha\beta}e_{\alpha\beta}$. The general form of the elastic free energy density is then given by

$$f = f_0 + \frac{1}{2}\lambda e_{\gamma\gamma}e_{\delta\delta} + \mu e_{\alpha\beta}e_{\alpha\beta}, \tag{2.19}$$

where λ, μ are called the Lamé coefficients and f_0 is a negligible constant. Substituting the decomposition from Eq. (2.17), we get:

$$f = \frac{K}{2}e_{\gamma\gamma}e_{\delta\delta} + \mu\bar{e}_{\alpha\beta}\bar{e}_{\alpha\beta}, \tag{2.20}$$

where $\bar{e}_{\alpha\beta} = e_{\alpha\beta} - \frac{1}{d}\delta_{\alpha\beta}e_{\gamma\gamma}$ represents the traceless part of the microscopic strain tensor. The constant $K = \lambda + 2\mu/d > 0$ is well known as the *bulk modulus* or modulus of compression, as is $\mu > 0$, the *shear modulus* or modulus of rigidity. Using the amplitudes $\tilde{u}(\mathbf{k})$ and the tensor $\mathbf{E}$ as independent degrees of freedom, we can write the elastic Hamiltonian of the system as follows:

$$\mathscr{H}_{\mathrm{el}} = \int_V \mathrm{d}^d\mathbf{r}\left(\frac{K}{2}e_{\gamma\gamma}e_{\delta\delta} + \mu\bar{e}_{\alpha\beta}\bar{e}_{\alpha\beta}\right). \tag{2.21}$$

Analogous to the microscopic strain tensor, the macroscopic strain tensor can also be decomposed into trace and traceless part:

$$E_{\alpha\beta} = \frac{1}{d}E_0\delta_{\alpha\beta} + \bar{E}_{\alpha\beta}, \tag{2.22}$$

where $E_0 = E_{\gamma\gamma}$ describes the change in volume. Using the Fourier expansion of $\mathbf{u}$, Eq. (2.13) and substituting it in the definition of $e_{\alpha\beta}$, Eq. (2.16), yields

$$e_{\alpha\beta} = E_{\alpha\beta} + \frac{\mathrm{i}}{2}\sum_{\mathbf{k}\neq 0}\sum_{\lambda=1}^{d-1}\exp(\mathrm{i}\mathbf{k}\cdot\mathbf{r})\tilde{u}^{(\lambda)}(\mathbf{k})\left(k_\alpha\epsilon_\beta^{(\lambda)} + k_\beta\epsilon_\alpha^{(\lambda)}\right), \tag{2.23}$$

as well as

$$e_{\gamma\gamma} = E_0 + \mathrm{i}\sum_{\mathbf{k}}\exp(\mathrm{i}\mathbf{k}\cdot\mathbf{r})k\tilde{u}^{(0)}(\mathbf{k}). \tag{2.24}$$

With the relation

$$\int_V \mathrm{d}^d\mathbf{r}\exp(\mathrm{i}(\mathbf{k}-\mathbf{q})\cdot\mathbf{r})) = V\delta_{\mathbf{kq}}, \tag{2.25}$$

the elastic Hamiltonian can finally be written as

$$\begin{aligned}\frac{\mathscr{H}_{\mathrm{el}}}{V} =& \frac{K}{2}E_0^2 + \mu\bar{E}_{\alpha\beta}\bar{E}_{\alpha\beta} \\ &+ \frac{1}{2}\left[K + 2\left(1-\frac{1}{d}\right)\mu\right]\sum_{\mathbf{k}}k^2\left|\tilde{u}^{(0)}(\mathbf{k})\right|^2 \\ &+ \frac{\mu}{2}\sum_{\mathbf{k}}\sum_{\lambda=1}^{d-1}k^2\left|\tilde{u}^{(\lambda)}(\mathbf{k})\right|^2.\end{aligned} \tag{2.26}$$

The first line in Eq. (2.26) accounts for macroscopic deformation in form of compression and shear. The second line gives the elastic energy of the longitudinal modes and the third line gives the energy of the transversal modes. From Eq. (2.26) we see, that longitudinal and transversal modes have different elastic constants: While the longitudinal modes depend both on bulk and shear modulus, the transversal modes depend only on the shear modulus. Also, for $d > 1$, the macroscopic compression exhibits a smaller elastic constant than the longitudinal modes. We define

$$K' = K + 2\left(1-\frac{1}{d}\right)\mu. \tag{2.27}$$

2.2.2 Order Parameter and Coupling Energy

For the magnetic interaction we will assume, that without coupling the system is described by a Landau-Ginzburg-Wilson Hamiltonian (see Sec. 2.1.):

$$\mathscr{H}_{\mathrm{LGW}} = \int \mathrm{d}^d\mathbf{r}\left(\frac{R}{2}(\boldsymbol{\nabla}\phi(\mathbf{r}))^2 + \frac{r_0}{2}\phi^2(\mathbf{r}) + \frac{u_0}{4!}\phi^4(\mathbf{r}) - H\phi(\mathbf{r})\right). \tag{2.28}$$

The order parameter $\phi(\mathbf{r})$ is a scalar field, which in Fourier space is represented by

$$\phi(\mathbf{r}) = \sum_{\mathbf{k}} \tilde{\phi}(\mathbf{k})\exp(\mathrm{i}\mathbf{k}\cdot\mathbf{r}) = \phi_0 + \sum_{\mathbf{k}\neq 0} \tilde{\phi}(\mathbf{k})\exp(\mathrm{i}\mathbf{k}\cdot\mathbf{r}). \tag{2.29}$$

With this, the LGW Hamiltonian can be transformed into Fourier space as well:

$$\begin{aligned}\frac{\mathscr{H}_{\mathrm{LGW}}}{V} =& \frac{R}{2}\sum_{\mathbf{k}} k^2\left|\tilde{\phi}(\mathbf{k})\right|^2 + \frac{r_0}{2}\sum_{\mathbf{k}}\left|\tilde{\phi}(\mathbf{k})\right|^2 \\ &+ \frac{u_0}{4!}\sum_{\mathbf{k}_1\mathbf{k}_2\mathbf{k}_3} \tilde{\phi}(\mathbf{k}_1)\tilde{\phi}(\mathbf{k}_2)\tilde{\phi}(\mathbf{k}_3)\tilde{\phi}(-\mathbf{k}_1-\mathbf{k}_2-\mathbf{k}_3).\end{aligned} \tag{2.30}$$

For the coupling energy, we will use the lowest order coupling compliant with the systems symmetries. For small fields $\phi(\mathbf{r})$ and small elastic distortions, the lowest order coupling is given by

$$\mathscr{H}_{\mathrm{c}} = g\int \mathrm{d}^d\mathbf{r}\,\phi^2(\mathbf{r})e_{\alpha\alpha}. \tag{2.31}$$

The parameter g determines the coupling strength. We use this form, because rotation invariance must be given and the trace is the only invariant scalar, which can be extracted from a second rank tensor. Also, the square of the order parameter must be used in order to provide for spin inversion symmetry. Next, consider the substitution $\phi^2 = \psi$, where ψ can again be expressed in terms of the Fourier transform

$$\psi(\mathbf{r}) = \sum_{\mathbf{k}} \tilde{\psi}(\mathbf{k})\exp(\mathrm{i}\mathbf{k}\cdot\mathbf{r}) = \psi_0 + \sum_{\mathbf{k}\neq 0} \tilde{\psi}(\mathbf{k})\exp(\mathrm{i}\mathbf{k}\cdot\mathbf{r}). \tag{2.32}$$

This can be used to rewrite the coupling Hamiltonian as

$$\frac{\mathscr{H}_{\mathrm{c}}}{V} = g\psi_0 E_0 + \mathrm{i}g\sum_{\mathbf{k}\neq 0} k\tilde{\psi}^*(\mathbf{k})\tilde{u}_0(\mathbf{k}). \tag{2.33}$$

From this form we see, that the shear component of macroscopic deformation $\bar{E}_{\alpha\beta}$ and the transversal elastic modes $\tilde{u}^{(\lambda)}$ with $0 < \lambda < d$ do not couple at all with the order parameter. Since both those quantities occur quadratically in the elastic Hamiltonian Eq. (2.26), they can be eliminated by Gaussian integration[1].

[1] This is possible, since all the relevant information is coded in the partition function $Z \propto \int \mathrm{d}\Gamma \exp(-\beta\mathscr{H}(\Gamma))$. A quadratic summand in the Hamiltonian will therefore result merely in a constant factor in the partition function and will not interfere with any thermodynamic averages.

We can then write the sum of elastic and coupling Hamiltonian as

$$\begin{aligned}\frac{\mathscr{H}_{\mathrm{el}}+\mathscr{H}_{\mathrm{c}}}{V} =& -\frac{g^2}{2K}\psi_0^2-\frac{g^2}{2K'}\sum_{\mathbf{k}\neq 0}\left|\tilde{\psi}(\mathbf{k})\right|^2+\frac{K}{2}\left(E_0+\frac{g}{K}\psi_0\right)^2 \\ &+\frac{K'}{2}\sum_{\mathbf{k}\neq 0}\left|k\tilde{u}_0(\mathbf{k})-\mathrm{i}\frac{g}{K'}\tilde{\psi}(\mathbf{k})\right|^2.\end{aligned} \tag{2.34}$$

It becomes clear, that like the transversal elastic fluctuations, the longitudinal fluctuations can be eliminated as well for analogous reasons. The last term can therefore be omitted completely. By incorporating the $\mathbf{k}=0$ modes into the sum, this can be rewritten as

$$\frac{\mathscr{H}_{\mathrm{el}}+\mathscr{H}_{\mathrm{c}}}{V} = -J\psi_0^2-\frac{g^2}{2K'}\sum_{\mathbf{k}}\left|\tilde{\psi}(\mathbf{k})\right|^2+\frac{K}{2}\left(E_0+\frac{g}{K}\psi_0\right), \tag{2.35}$$

where a coupling parameter

$$J=\frac{g^2}{2}\left(\frac{1}{K}-\frac{1}{K'}\right)>0 \tag{2.36}$$

was introduced. Since

$$\sum_{\mathbf{k}}\left|\tilde{\psi}(\mathbf{k})\right|^2=\frac{1}{V}\int \mathrm{d}^d\mathbf{r}\,\psi^2(\mathbf{r})=\frac{1}{V}\int \mathrm{d}^d\mathbf{r}\,\phi^4(\mathbf{r}), \tag{2.37}$$

the second term of Eq. (2.35) can be absorbed in the LGW Hamiltonian with a redefinition of the parameter u_0:

$$\frac{u_0}{4!}\to\frac{u}{4!}=\frac{u_0}{4!}-\frac{g^2}{2K'}. \tag{2.38}$$

This means, that depending on the strength of the coupling g, the parameter u will be positive or negative. As we will see later, this will have an important effect on the nature of the phase transition. With the reparametrization $\mathscr{H}_{\mathrm{LGW}}\to\mathscr{H}'_{\mathrm{LGW}}$, the effective Hamiltonian of the system is given by

$$\frac{\mathscr{H}}{V}=\frac{\mathscr{H}'_{\mathrm{LGW}}}{V}-J\left(\sum_{\mathbf{k}}\left|\tilde{\phi}(\mathbf{k})\right|^2\right)^2+\frac{K}{2}\left(E_0+\frac{g}{K}\sum_{\mathbf{k}}\left|\tilde{\phi}(\mathbf{k})\right|^2\right)^2. \tag{2.39}$$

In the case of *constant pressure*, the volume and therefore the trace of the macroscopic strain tensor E_0, is allowed to fluctuate. The last term of the effective Hamiltonian can then again be eliminated by Gaussian integration, leaving a coupling term with $J>0$ as defined in Eq. (2.36).

In the case of *constant volume*, E_0 is constant as well and the square bracket in the last term can be expanded. First, this yields a constant term proportional to E_0^2, which can be omitted right away. The second term is proportional to $\sum_{\mathbf{k}}\left|\tilde{\phi}(\mathbf{k})\right|^2$ and can be absorbed in $\mathscr{H}'_{\mathrm{LGW}}$ with the reparametrization

$$r_0\to r=r_0+E_0 g, \tag{2.40}$$

which just corresponds to a shift in critical temperature. The third and last term is proportional to $\left(\sum_{\mathbf{k}} \left|\tilde{\phi}(\mathbf{k})\right|^2\right)^2$ and can be absorbed in a redefinition of the coupling constant

$$J = -\frac{g^2}{K'} < 0, \tag{2.41}$$

which in this case is smaller than zero, since $K' > 0$ (see Eq. (2.27)). This means, that for both constant pressure and constant volume an effective Hamiltonian

$$\frac{\mathcal{H}}{V} = \frac{\mathcal{H}'_{\mathrm{LGW}}}{V} - J\left(\sum_{\mathbf{k}} \left|\tilde{\phi}(\mathbf{k})\right|^2\right)^2 \tag{2.42}$$

remains, where $J > 0$ for $p = \text{const.}$ and $J < 0$ for $V = \text{const.}$

Before distinguishing between the two cases, we will discuss the case of *strong coupling*. As stated above, a large coupling g will lead to a negative coefficient u in $\mathcal{H}'_{\mathrm{LGW}}$. In order to allow for stable solutions, the Landau expansion in the order parameter must then be carried out up to sixth order, which then in turn must have a positive coefficient. It is well known, that this form produces a first order phase transition (see e.g. [11]). This becomes evident by looking

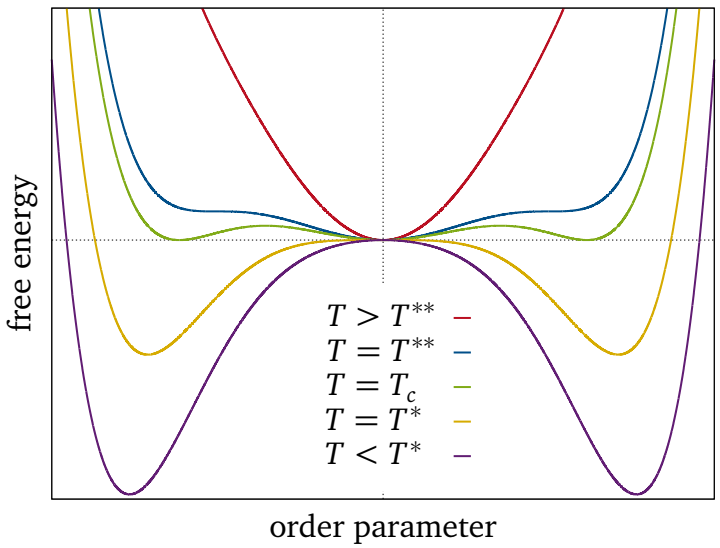

Figure 2.5: Landau free energy for different temperatures. The fourth order coefficient u is negative and the power series expansion therefore carried out up to sixth order.

at the temperature dependence of the Landau free energy (see Fig. 2.5): Coming from high temperatures, two local minima start to form as T passes a certain temperature T^{**}. These minima become global at $T = T_c^{\mathrm{MF}}$. This corresponds to the typical jump of the order parameter in first order phase transitions. At this point, there are three phases, that minimize free energy: $\phi = 0$ and $\phi = \pm\phi_{\mathrm{sp}}$. This corresponds to a triple point in the H-T diagram at $H = 0$. As temperature decreases further, only two phases $\pm\phi_{\mathrm{sp}}$ remain.

Assuming, that fluctuations in the order parameter are small, the interfacial energy term in $\mathcal{H}'_{\mathrm{LGW}}$ can be neglected. On these grounds, we can transfer the behavior described above to the present case. This means, that a *first order phase transition* is expected for strong coupling, regardless of the sign of J.

For weak coupling though, one has to differentiate between the cases $J > 0$ for constant pressure and $J < 0$ for constant volume.

2.2.3 Constant Pressure or $J > 0$

For the case of constant pressure, we start by examining the partition function, which is defined by the functional integral

$$Z \propto \int \mathscr{D}\phi \exp(-\beta \mathscr{H}(\phi)), \tag{2.43}$$

with $\beta = 1/(k_B T)$. We use the Hubbard-Stratonovic transformation

$$\sqrt{\frac{\pi}{a}} \exp\left(\frac{b^2}{4a}\right) = \int_{-\infty}^{\infty} \mathrm{d}x \exp\left(-ax^2 - bx\right) \tag{2.44}$$

with $a > 0$, in order to reduce the fourth order interaction in Eq. (2.42) to second order. This in return gives us an additional variable x. Now the partition function can be written as

$$Z \propto \int_{-\infty}^{\infty} \mathrm{d}x \int \mathscr{D}\phi \exp\left(-\beta \mathscr{H}_{\mathrm{LGW}}(r) - \frac{x^2}{4\beta V J} - x \sum_{\mathbf{k}} \left|\tilde{\phi}(\mathbf{k})\right|^2\right), \tag{2.45}$$

where the argument r of $\mathscr{H}_{\mathrm{LGW}}$ denotes the parameter in Landau expansion and not distance.

The remaining ϕ-dependent term can again be absorbed in $\mathscr{H}_{\mathrm{LGW}}$, leaving us with

$$Z \propto \int_{-\infty}^{\infty} \mathrm{d}x \int \mathscr{D}\phi \exp\left(-\beta \mathscr{H}_{\mathrm{LGW}}\left(r + \frac{2}{\beta V} x\right) - \frac{x^2}{4\beta V J}\right). \tag{2.46}$$

In the next step, we use the free energy density $f_0(r)$ from the undisturbed LGW system, from which we know at least the asymptotic critical behavior. The integration over ϕ can then be carried out yielding

$$Z \propto \int_{-\infty}^{\infty} \mathrm{d}x \exp\left(-\beta V f_0\left(r + \frac{2}{\beta V} x\right) - \frac{x^2}{4\beta V J}\right). \tag{2.47}$$

We now transform to the deviation from criticality with $y = r + 2x/(\beta V) - r_c$, where r_c is the value of r, at which $\mathscr{H}_{\mathrm{LGW}}$ is critical. With $f(y) = f_0(r + 2x/(\beta V)) = f_0(y + r_c)$ this gives us

$$Z \propto \int_{-\infty}^{\infty} \mathrm{d}y \exp\left(-\beta V f(y) - \frac{\beta V}{16J}(y - r + r_c)^2\right). \tag{2.48}$$

Since the integration only extends to one variable, we can in thermodynamic limit find the solution by just minimizing the free energy

$$f(y) + \frac{1}{16J}(y - r + r_c)^2 \stackrel{!}{=} \min. \tag{2.49}$$

This can be done by finding the root of the derivative:

$$-8J f'(y) = y - r + r_c. \tag{2.50}$$

Near criticality, f will have the form $f(y) = -A|y|^{2-\alpha}$, where $A > 0$ is a critical amplitude and α is the critical exponent of the specific heat in the original LGW system. Here, only $\alpha > 0$ is considered. This is the case, if $\mathscr{H}_{\mathrm{LGW}}$ describes the rigid Ising model in $d = 3$ dimensions. We receive

$$g(y) := 8JA(2-\alpha)|y|^{1-\alpha}\mathrm{sign}(y) = y - r + r_c. \tag{2.51}$$

The left hand side flattens out with weakening coupling J. The right hand side is just a line with slope 1 going through the origin for $T = T_c$. It is shifted downward for $T > T_c$ and upward for $T < T_c$. A solution can be obtained by finding the points of intersection graphically, as illustrated in Fig. 2.6. There is exactly one solution for high and low temperatures, whereas

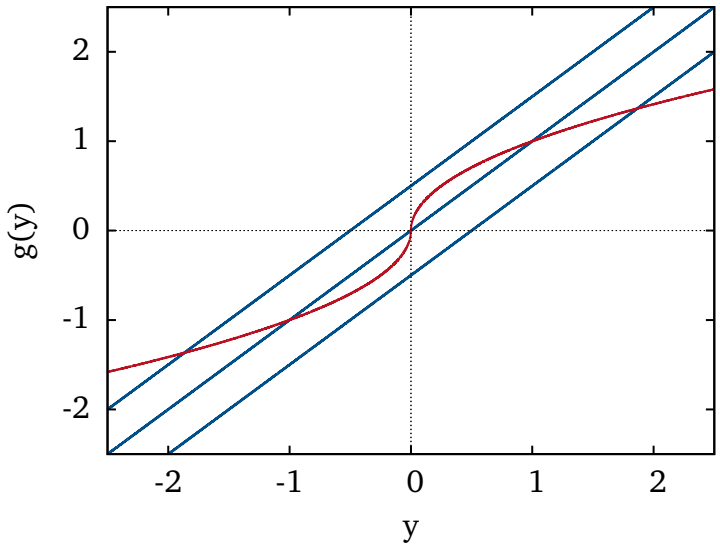

Figure 2.6: Graphical solution of Eq. (2.51) for $J > 0$ in arbitrary units. The blue lines are the right hand side for different temperatures. The red curve is the left hand side $g(y)$.

near the critical temperature there are three solutions.

A solution y is only then stable, if it corresponds to a minimum of the free energy and not a maximum. This is the case, if the second derivative of Eq. (2.49) is bigger than zero, i.e.

$$f''(y) + \frac{1}{8J} > 0. \tag{2.52}$$

Since $g(y) = -8Jf'(y)$, we can alternatively demand $g'(y) < 1$. This means, that a solution is stable, if the slope of g is less than the slope of the line at the point of intersection. This holds for both solutions on the outside, but not for the one in the center. As temperature passes T_c the system jumps from one solution to the other corresponding to a *first order phase transition*.

2.2.4 Constant Volume or $J < 0$

For the case of constant volume it is assumed, that it is possible to analytically extend the method above with respect to $J < 0$. This is quite daring, but will yield the same results as renormalization group techniques [6, 7]. The first step is again the graphical solution of Eq.

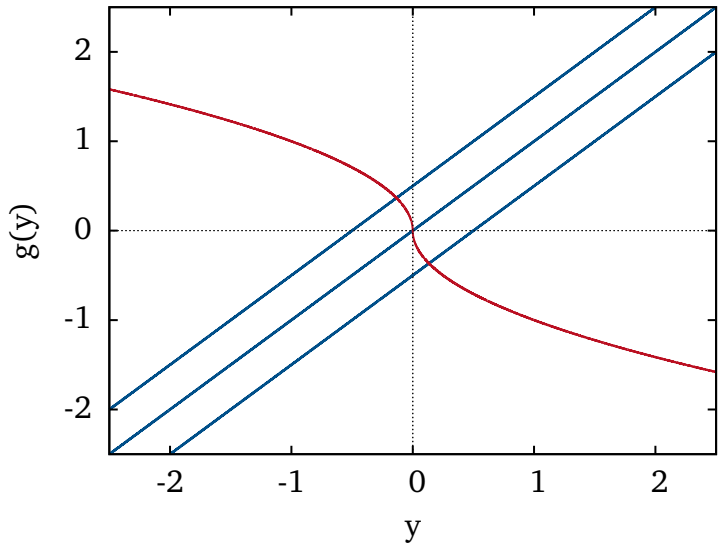

Figure 2.7: Graphical solution of Eq. (2.51) for $J < 0$ in arbitrary units. The blue lines are the right hand side for different temperatures. The red curve is the left hand side $g(y)$.

(2.51), as illustrated in Fig. 2.7. After the analytical continuation, the stability criterion will be different, but since in any case there is only one solution anyway, this is of no concern. We will therefore expect a *second order phase transition*. By expanding Eq. (2.51) up to leading order, we find, that near the critical point

$$y \propto |r - r_c|^{1/(1-\alpha)} \tag{2.53}$$

holds. This relation is the subject of Fisher's hidden variable theory [3]. His analysis predicts *Fisher renormalized critical exponents*

$$\beta_F = \frac{\beta}{1-\alpha}, \tag{2.54}$$

$$\nu_F = \frac{\nu}{1-\alpha}, \tag{2.55}$$

$$\gamma_F = \frac{\gamma}{1-\alpha}, \tag{2.56}$$

$$\alpha_F = -\frac{\alpha}{1-\alpha}. \tag{2.57}$$

The most distinct sign of Fisher renormalization is the change of sign of the specific heat exponent α. This means, that the specific heat will no longer diverge at the critical point, but form a cusp singularity. The existence of Fisher renormalized exponents has been confirmed by simulation by A. Tröster [9]. In his work, he uses a similar effective Hamiltonian without microscopic elastic fluctuations.

2.3 Scaling Principles

Second order phase transitions are always connected with the divergence of a correlation length ξ. In the case of the Ising model this is the spin-spin correlation length ξ. The divergence of ξ is of course only possible in the thermodynamic limit $N \to \infty$. In a finite system however, the correlation length is bounded by the linear system size L. As a consequence, critical divergences are rounded and shifted over some region in temperature. As $N \to \infty$, the width of this region smoothly converges to zero. The finite-size scaling method makes use of the fact, that the smearing of the phase transition in finite systems occurs by well defined systematics. In the following, critical exponents are motivated and a number of scaling relations are derived. Most of the following derivations are taken from [14].

2.3.1 Critical Exponents

In simulation, the divergence of the correlation length corresponds to the growth of a cluster with constant order parameter. A critical cluster has only two natural length scales: The microscopic scale a (e.g. the lattice constant) and the linear box size L, which is the maximum cluster size possible. Consider now a system in the infinite size limit, where the scales L and a play no role. When there is no natural length scale, the sample must look the same, regardless of the degree of magnification. This is a property of self-similarity and therefore leads to power law behavior.

For two spins S_i and S_j at distance r and in the vicinity of the critical point, the correlation function is denoted by $G(r) = \langle S_i S_j \rangle$. If we scale the distance r by a factor $\lambda > 1$, the correlation function scales as

$$G(\lambda r) = \phi(\lambda, r) G(r), \tag{2.58}$$

where ϕ is the *rescaling function*. Of course $\phi(1, r) = 1$. Since λ and ϕ are dimensionless, ϕ cannot depend on r. If this were the case, there had to be another length scale ζ, such that r/ζ would result in a dimensionless value. By definition of criticality, such a length scale cannot exist, and therefore ϕ is independent of r. By repeated application of Eq. (2.58) one easily sees, that

$$\phi(\lambda\mu) = \phi(\lambda)\phi(\mu). \tag{2.59}$$

Taking the logarithmic derivative with respect to μ yields

$$\lambda \frac{\phi'(\lambda\mu)}{\phi(\lambda\mu)} = \frac{\phi'(\mu)}{\phi(\mu)}. \tag{2.60}$$

Setting $\mu = 1$ and using $\phi(1) = 1$ gives us then

$$\phi'(\lambda) = \phi'(1) \frac{\phi(\lambda)}{\lambda} \propto \frac{\phi(\lambda)}{\lambda}. \tag{2.61}$$

This means, that the rescaling function ϕ must have the form of a *power law*. We then define the critical exponent η by

$$\phi(\lambda) = \lambda^{-(d-2+\eta)}, \tag{2.62}$$

where d is the spatial dimension of the system. By setting $\lambda = a/r$ we find, that

$$G(r) \propto r^{-(d-2+\eta)} \tag{2.63}$$

at criticality.

Considering the *reduced temperature*

$$t = 1 - \frac{T}{T_c}, \tag{2.64}$$

similar arguments hold: Near the critical point, there should be no particular nonzero values of t, that are characteristic of the system. This leads to the power-law relation for the correlation length

$$\xi(t) \propto |t|^{-\nu}. \tag{2.65}$$

Away from the critical point, the correlation function G should only depend on the ratio r/ξ. We therefore write

$$G(r, \xi) = r^{-(d-2+\eta)} \tilde{G}\left(\frac{r}{\xi}\right), \tag{2.66}$$

with $\tilde{G} \to$ const. as $r/\xi \to 0$. This way, $\tilde{G}$ can be seen as a measure of the deviation from the critical case given by Eq. (2.63). We use this as basis to derive the other critical exponents via scaling laws.

Consider the magnetization m, which is defined by

$$m = L^{-d} \sum_i S_i. \tag{2.67}$$

The magnetic susceptibility χ is related to the magnetization m by the fluctuation relation

$$\chi = \frac{L^d}{k_B T} \left(\left\langle m^2 \right\rangle - \langle m \rangle^2 \right), \tag{2.68}$$

where L is the linear size of the system. Alternatively, the susceptibility can be obtained by

$$\chi \propto \int \mathrm{d}^d \mathbf{r}\, G(r, \xi). \tag{2.69}$$

We can use the factorization of the correlation function Eq. (2.66), to solve the integral by transforming to r/ξ:

$$\begin{aligned} \chi &\propto \int \mathrm{d}^d \mathbf{r}\, r^{-(d-2+\eta)} \tilde{G}\left(\frac{r}{\xi}\right) \\ &\propto \int_0^\infty \mathrm{d}r\, r^{1-\eta} \tilde{G}\left(\frac{r}{\xi}\right) \\ &= \xi^{2-\eta} \int_0^\infty \mathrm{d}x\, x^{1-\eta} \tilde{G}(x). \end{aligned} \tag{2.70}$$

Near criticality, this gives us the scaling relation of the susceptibility

$$\chi \propto \xi^{2-\eta} \propto |t|^{-\nu(2-\eta)}, \tag{2.71}$$

with the critical exponent

$$\gamma = \nu(2-\eta). \tag{2.72}$$

This conveys, that the divergence in susceptibility at the critical point is generated from the increasing range of spin-spin correlations.

Now consider two spins S_i and S_j at a distance $r \gg \xi$. The correlation between them is approximately the same as the magnetic correlation of two spin subblocks of size ξ^d:

$$\langle S_i S_j \rangle \approx \langle m_I m_J \rangle, \tag{2.73}$$

where

$$m_I = \frac{a^d}{\xi^d} \sum_{i \in I} S_i. \tag{2.74}$$

I denotes a set of spins within a region in space of the size of the correlation volume. If we scale $\xi \to \lambda\xi$ and $r \to \lambda r$ such that ξ/λ remains constant, the correlation function scales as $G \to \lambda^{-(d-2-\eta)} G$. For consistency reasons, the magnetization must rescale like $m_I \to \lambda^{-(d-2+\eta)/2} m_I$. This must not only hold for a correlation volume, but also for the system as a whole:

$$m(\lambda\xi) = \lambda^{-(d-2+\eta)/2} m(\xi). \tag{2.75}$$

By setting $\lambda = a/\xi$, we obtain the scaling relation

$$m \propto \xi^{-(d-2+\eta)/2} \propto |t|^{\nu(d-2+\eta)/2}. \tag{2.76}$$

This yields the critical exponent of magnetization

$$\beta = \nu(d-2+\eta)/2\,. \tag{2.77}$$

Eq. (2.77) is a *hyperscaling relation*, as are all relations involving the spacial dimension d. Hyperscaling relations are only valid at and below a critical upper dimension d_c. For higher dimensions, hyperscaling, and therefore the standard finite-size scaling apparatus, is not valid. In the Ising model, as well as in ϕ^4 theories in general, $d_c = 4$.

For the derivation of the critical exponent of the specific heat, we argue that the free energy of a correlation volume should be of order $k_B T$:

$$F \propto \frac{L^d}{\xi^d} k_B T \tag{2.78}$$

This means, that for the free energy per volume

$$f = L^{-d} F \propto \xi^{-d} \propto |t|^{d\nu} \tag{2.79}$$

holds. Taking twice the derivative with respect to t gives the relation for the critical exponent of heat capacity

$$\alpha = 2 - d\,\nu, \tag{2.80}$$

a hyperscaling relation as well.

2.3.2 Finite-Size Scaling

The idea of finite-size scaling strongly relies on the order parameter probability density function $P(m)$. The exact expectation value of the magnetization is always zero in finite systems, since P is symmetric around $m = 0$ (See Fig. 2.8):

$$\langle m \rangle = \int \mathrm{d}m \, m P(m, T, L) = 0. \tag{2.81}$$

This is another consequence of the fact, that phase transitions can only happen in the thermodynamic limit. Below T_c there are two equivalent ordered phases with the spontaneous magnetizations $m = \pm m_\mathrm{sp}(T)$. In a system of finite-size, there are always states connecting both ordered phases, allowing the system to go from one phase to the other. For increasing system size L, the statistical weight of those connecting states becomes less until they vanish completely in the thermodynamic limit. This means the system is then trapped in one of the two equivalent ordered states. Well below T_c the two peaks centered around $\pm m_\mathrm{sp}$ are described in good approximation by Gaussians. This is, because for $\xi \ll L$ we can consider the system to be a large sum of independent parts and apply the Central Limit Theorem [15]:

$$P(m) = \frac{1}{2}\sqrt{\frac{L^d}{2\pi k_\mathrm{B} T \chi'}}\left[\exp\left(-\frac{L^d (m - m_\mathrm{sp})^2}{2 k_\mathrm{B} T \chi'}\right) + \exp\left(-\frac{L^d (m + m_\mathrm{sp})^2}{2 k_\mathrm{B} T \chi'}\right)\right]. \tag{2.82}$$

Here we introduced the finite-lattice susceptibility[2]

$$\chi' = \frac{L^d}{k_\mathrm{B} T}\left(\left\langle m^2 \right\rangle - \langle |m| \rangle^2\right). \tag{2.83}$$

For $T \gg T_\mathrm{c}$, there is only one phase with $m = 0$ and the probability density is in good approximation a *single Gaussian* for analogous reasons. In Fig. 2.8 there are some example probability density functions sampled from simulation at different temperatures.

For the scaling behavior of $P(m, \xi, L)$ we can make some general assumptions. One consideration is, that a dilation of the correlation length $\xi \to \lambda\xi$ (from now on ξ is always the correlation length of the corresponding infinite system) can be compensated by scaling the system size like $L \to \lambda L$. After this transformation it should be equally likely to find a magnetization m in the original system, as it is to find a magnetization $\lambda^{-\beta/\nu} m$ in the new system:

$$P(m, \xi, L)\,\mathrm{d}m = P\left(\lambda^{-\beta/\nu} m, \lambda\xi, \lambda L\right) \mathrm{d}\left(\lambda^{-\beta/\nu} m\right). \tag{2.84}$$

With the choice $\lambda = a/L$ this becomes

$$P(m, \xi, L) = L^{\beta/\nu} \tilde{P}\left(L^{\beta/\nu} m, \xi/L\right), \tag{2.85}$$

[2] The regular, infinite lattice susceptibility is defined as $\chi = L^d\left(\left\langle m^2 \right\rangle - \langle m \rangle^2\right)/k_\mathrm{B} T$. Since this is zero in finite systems, we use the alternative definition with the symmetrized order parameter.

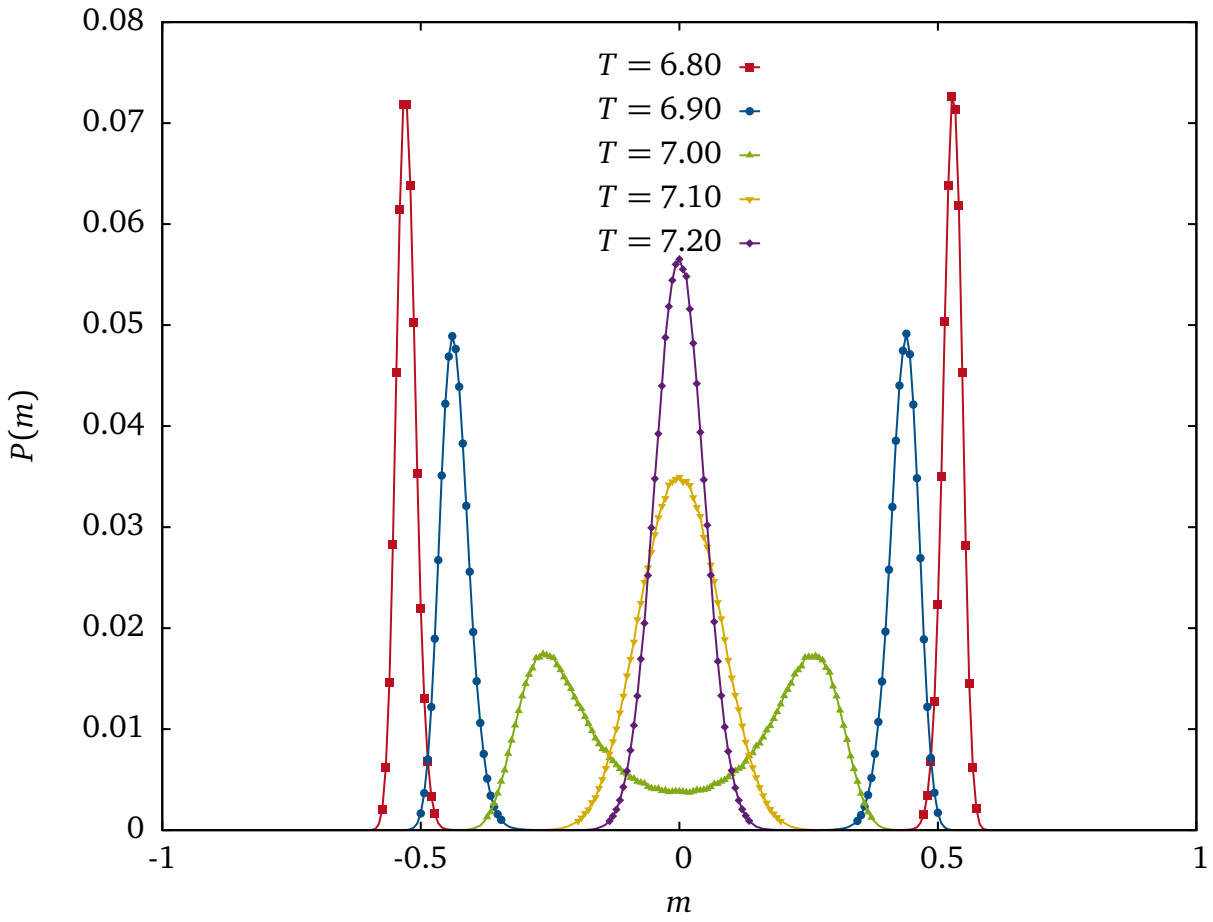

Figure 2.8: Histograms of the magnetization m at $L = 48$, $\kappa = 1$, $K = 3$ and different temperatures above and below $T_c \approx 7.01$.

where $\tilde{P}$ is a scaling function much like $\tilde{G}$ in Eq. (2.66). This can then be used to derive the relation

$$\begin{aligned}\left\langle |m|^k \right\rangle &= \int \mathrm{d}m\, |m|^k P(m, \xi, L) \\ &= L^{-k\beta/\nu} \tilde{\mu}_k(\xi/L) \\ &= L^{-k\beta/\nu} \tilde{\mu}_k\left(L^{1/\nu} t\right)\end{aligned} \tag{2.86}$$

for the scaling behavior of the magnetic moments. From this follows for the susceptibility:

$$\begin{aligned}\chi' &= L^{d-2\beta/\nu} \tilde{\chi}'\left(L^{1/\nu} t\right) \\ &= L^{\gamma/\nu} \tilde{\chi}'\left(L^{1/\nu} t\right).\end{aligned} \tag{2.87}$$

In the same way, a relation for the specific heat

$$C = L^{-d} (k_\mathrm{B} T)^{-2} \left(\left\langle E^2 \right\rangle - \langle |E| \rangle^2\right), \tag{2.88}$$

can be obtained. By examining the probability density function of the energy we find, that

$$C = L^{\alpha/\nu} \tilde{C}\left(L^{1/\nu} t\right). \tag{2.89}$$

In addition to the rounding of critical divergences, finite-size effects include a shift in critical temperature. For the estimation of the size dependent critical temperature the point of steepest descent of the magnetic moments or the point of maximum susceptibility/specific heat can be used. In fact, the distance from the actual critical temperature scales as

$$T_\mathrm{c}(L) - T_\mathrm{c} \propto L^{-1/\nu}. \tag{2.90}$$

2.4 Multi Histogram Reweighting

With the multi histogram reweighting method, the information of one or more simulations at given temperatures can be combined in order to compute observables on a continuous range of temperatures (see Fig. 2.9). This is a great way to extract the maximum amount of information

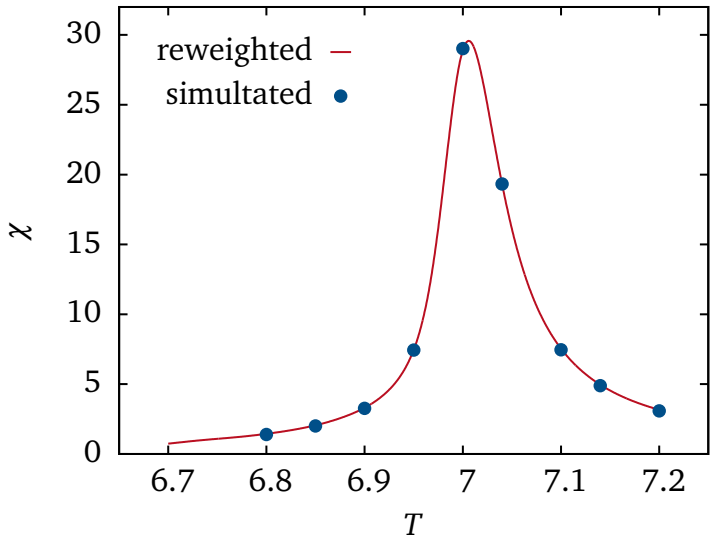

Figure 2.9: Reweighting of the magnetic susceptibility χ. The susceptibility diverges at the critical point in the thermodynamic limit. Here, however, the divergence is rounded off due to finite-size effects.

possible from given Monte-Carlo simulations. The method was popularized by Ferrenberg and Swendsen in the late 1980s [16, 17] although the idea itself is much older.

Consider n simulations at inverse temperature β_i and number of Monte-Carlo steps N_i. The *true* probability density function of energy E and magnetization m in each system is given by

$$P_i(m,E) = D(m,E)\exp(-\beta_i E + f_i), \tag{2.91}$$

where the density of states $D(m,E)$ is independent of β. The f_i are the dimensionless free energies and related to the partition function Z_{β_i} by

$$f_i = \beta_i F_i = -\log\left(Z_{\beta_i}\right). \tag{2.92}$$

If we have histograms $H_i(m,E)$ with $H \in \mathbb{N}$ and m, E discrete, we can approximate the true distribution by

$$P_i(m,E) \approx \frac{H_i(m,E)}{N_i}. \tag{2.93}$$

The simulations will give us estimates of $D(m,E) = P_i(m,E)\exp(\beta_i E - f_i)$ at different ranges of E since they were performed at different β. We estimate the density of states by performing a weighted average over the individual simulations:

$$D(m,E) \approx \sum_{i=1}^{n} w_i(m,E)\frac{H_i(m,E)}{N_i}\exp(\beta_i E - f_i), \tag{2.94}$$

where the weights w_i must satisfy

$$\sum_{i=1}^{n} w_i(m,E) = 1 \tag{2.95}$$

for all E and m. The exact weights are then obtained by minimizing the error $\sigma^2(D(m,E))$. For long enough simulations and narrow enough bin widths, it is reasonable to assume, that the values $H_i(m,E)$ of the histograms are Poisson distributed around their real value $\bar{H}_i(m,E)$. The error of $H_i(m,E)$ is therefore given by

$$\sigma^2(H_i(m,E)) = g_i \bar{H}_i(m,E) \approx g_i N_i D(m,E) \exp(-\beta_i E + f_i), \tag{2.96}$$

where $g_i = (1 + 2\tau_i)$ and τ_i the autocorrelation time of run i. Accordingly, the error in $D(E)$ can be written as

$$\begin{aligned} \sigma^2(D(m,E)) &= \sum_{i=1}^{n} w_i^2(m,E) \frac{\sigma^2(H_i(m,E))}{N_i^2} \exp(2(\beta_i E - f_i)) \\ &\approx \sum_{i=1}^{n} w_i^2(m,E) \frac{g_i}{N_i} D(m,E) \exp(\beta_i E - f_i). \end{aligned} \tag{2.97}$$

In order to minimize $\sigma^2(D(m,E))$ with respect to the w_i, we can use Lagrange multipliers λ and solve

$$\nabla_{\mathbf{w},\lambda} \left(\sigma^2(D(m,E)) - \lambda \left(\sum_{j=1}^{n} w_j(m,E) - 1 \right) \right) = 0. \tag{2.98}$$

This yields

$$w_i(m,E) = \frac{\lambda}{2} \frac{N_i}{g_i D(m,E)} \exp(-\beta_i E + f_i), \tag{2.99}$$

$$\lambda = \frac{2}{\sum_j \frac{N_j}{g_j D(m,E)} \exp\left(-\beta_j E + f_j\right)}. \tag{2.100}$$

Combining the above equations gives us for the weights

$$w_i(m,E) = \frac{N_i \exp(-\beta_i E + f_i)/g_i}{\sum_j N_j \exp\left(-\beta_j E + f_j\right)/g_j}. \tag{2.101}$$

With this, the density of states can be written as:

$$D(m,E) = \frac{\sum_{i=1}^{n} H_i(m,E)/g_i}{\sum_{j=1}^{n} N_j \exp\left(-\beta_j E + f_j\right)/g_j}. \tag{2.102}$$

The free energies f_i are at this point undetermined. By using Eq. (2.91) with $\sum_{m,E} P_i(m,E) = 1$ we find, that

$$\begin{aligned} f_i &= -\log\left(\sum_{m,E} D(m,E)\exp(-\beta_i E)\right) \\ &= -\log\left(\sum_{m,E} \frac{\sum_{k=1}^{n} H_k(m,E)/g_k}{\sum_{j=1}^{n} N_j \exp\big((\beta_i-\beta_j)E + f_j\big)/g_j}\right), \end{aligned} \tag{2.103}$$

which can be solved iteratively. One can usually start by setting $f_i = 0$ for all i and get a better approximation by evaluating Eq. (2.103). This is then repeated with the new values, until the desired precision is reached. Note, that the f_i are only determined up to an additive constant[3], as we can see from Eq. (2.103). Knowing the f_i, the expectation value of an observable O at reweighted β can computed by

$$\langle O\rangle_\beta = \frac{\sum_{m,E} O(m,E)D(m,E)\exp(-\beta E)}{\sum_{m,E} D(m,E)\exp(-\beta E)}. \tag{2.104}$$

If the β_i are within a narrow interval, the correlation time can be considered to be approximately constant and the g_i thus cancel out in Eq. (2.103).

Reweighting to arbitrary temperature could only be done, if the histograms had infinite precision (in fact, in this case only one histogram would suffice). If we move away from the simulated temperatures, the tails of the histograms become increasingly important and the statistics therefore worse. As a rule of thumb, the histograms should not lie apart much further than one standard deviation.

Numerical Considerations

Since the exponential terms can quickly become quite big, some numerical precautions must be taken. For example, one should only compute the logarithmic quantities if possible. Consider the sum

$$S = \sum_{i=1}^{N} \mathrm{e}^{a_i}. \tag{2.105}$$

For large a_i, the individual terms may very quickly exceed the maximum size of a `double` variable. With $\hat{a} = \max_i a_i$, we can rewrite the sum as

$$S = \mathrm{e}^{\hat{a}} \sum_{i=1}^{N} \mathrm{e}^{a_i - \hat{a}}. \tag{2.106}$$

The worst-case scenario is now merely, that some of the summands become zero. Taking the logarithm gives us now

$$\log(S) = \hat{a} + \log\left(\sum_{i=1}^{N} \mathrm{e}^{a_i-\hat{a}}\right). \tag{2.107}$$

[3] Usually, one just sets $f_0 = 0$ and determines the remaining free energies accordingly.

It is always a good idea to sort the a_i in ascending order beforehand. This way the small terms will be summed up first avoiding rounding errors. Under this requirement we can now write

$$\log(S) = \hat{a} + \log\left(1 + \sum_{i=1}^{N-1} \mathrm{e}^{a_i - \hat{a}}\right). \tag{2.108}$$

There usually exist special functions to compute $\log(1 + x)$ for small x with better performance and precision as compared to the standard logarithm. This so called *log-sum-exp* method can easily be automated with a function. In C we can for example define:

```
double logsumexp(double *exponents, int length)
{
    int i;
    double delta;
    long double q = 0.;

    /* sort array in ascending order */
    qsort(exponents, length, sizeof(double), compare);

    for(i = 0; i < length - 1; ++i)
    {
        delta = exponents[i] - exponents[length - 1];
        q += expl(delta);
    }
    return exponents[length - 1] + log1pl(q);
}
```

2.5 Error Analysis

Monte Carlo simulations with algorithms like the Metropolis or Swendsen-Wang algorithm can be represented by Markov Chains and therefore produce correlated data. Averages obtained from such simulations are random variables for which Gaussian error analysis (which assumes independency) does not apply. Therefore, special tools are necessary in order to obtain correct estimates for their standard deviation. One popular tool for this purpose is the so called *blocking method*, as described by Flyvberg and Petersen in [18]. Consider a simulation with a length of n steps and measurements x_i, $i = 1, \ldots, n$. By the blocking transformation, the size of the data set is halved by combining two consecutive measurements to one block:

$$x_i' = \frac{1}{2}(x_i + x_{i+1}), \tag{2.109}$$

$$n' = \frac{n}{2}. \tag{2.110}$$

It is immediately clear, that the mean value $\bar{x}$ is conserved under this transformation:

$$\bar{x}' = \bar{x}. \tag{2.111}$$

As estimator for the standard deviation we use the function

$$c(x) = \frac{1}{n(n-1)} \sum_{i=1}^{n} (x_i - \bar{x})^2. \tag{2.112}$$

By repeated application of the blocking transformation, the block size increases and eventually exceeds the correlation time τ. The estimator c then approaches the real value σ^2 of the variance, resulting in a plateau as it is shown in Fig. 2.10.

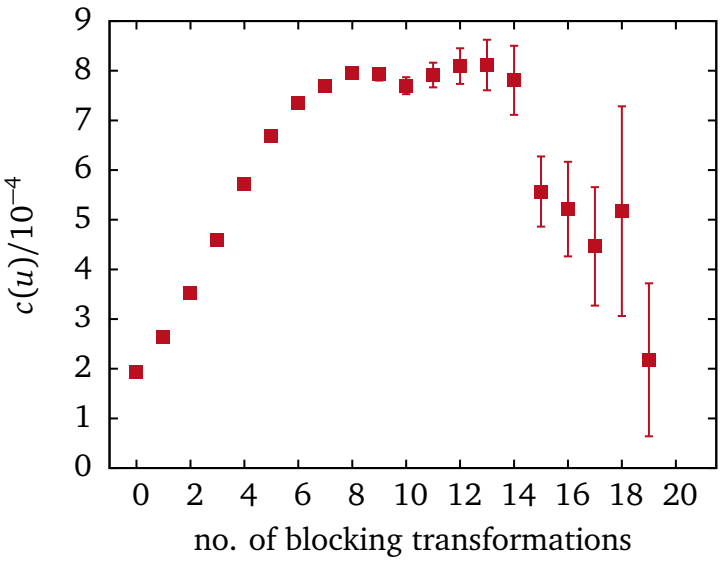

Figure 2.10: Error analysis for the internal energy u. From the plot we can estimate, that $\sigma^2(u) \approx 8 \cdot 10^{-4}$.

At this point the blocked measurements x_i' can be considered independent and even a standard deviation of the estimate c can be estimated:

$$\sigma(\bar{x}) \approx \sqrt{\frac{1}{n'(n'-1)} \sum_{i=1}^{n'} \left(x_i' - \bar{x}\right)^2} \left(1 \pm \frac{1}{\sqrt{2(n'-1)}}\right). \tag{2.113}$$

If a plateau of $c(x')$ is not reached for $n' = 2$ the simulation is too short (even shorter than the correlation time).

2.6 Swendsen-Wang Algorithm

For a local update algorithm, like the Metropolis algorithm, the order parameter correlation time will behave like $\tau \propto \xi^z$, where $z \approx 2$ is called the dynamic critical exponent [19]. Since in finite systems the correlation length is limited by L, we have

$$\tau \propto L^z \tag{2.114}$$

near criticality. This means, that changes propagate diffusely. As a consequence, the CPU time needed to create an independent configuration scales as L^{z+d}. Below T_c, the phases separate and the correlation time even scales exponentially with

$$\tau \propto \exp\left(\frac{\Delta F}{k_B T}\right), \tag{2.115}$$

where $\Delta F \propto L^{d-1}$ is the interfacial free energy between the separate phases [14]. Hence it is very costly in terms of computation time, to obtain adequate statistics for large systems with local update algorithms.

In order to overcome these limitations, we can use non-local cluster algorithms like the Swendsen-Wang (SW) algorithm, as it is described for the q-state Potts model in [20, 21]. It was found, that with the SW algorithm the correlation time only scales as [22]

$$\tau \propto \log(L). \tag{2.116}$$

In the following we will show, that the SW algorithm is not only valid for the regular Ising model, which is equivalent to the $q = 2$ Potts model, but also for the model used in the present work.

The Hamiltonian of the simulated system has the general form

$$\mathcal{H} = \sum_{\langle ij \rangle} \big(V(r_{ij}) - J(r_{ij}) S_i S_j\big), \tag{2.117}$$

where V denotes an arbitrary potential depending only on r_{ij}. This means, that the probability density of a configuration $(\{S\}, \{\mathbf{r}\})$ is given by

$$\begin{aligned} P(\{S\},\{\mathbf{r}\}) &= \frac{1}{Z}\exp(-\beta\mathcal{H}) \\ &= \frac{1}{Z}\exp\left(-\beta\sum_{\langle ij\rangle}\big(V(r_{ij}) - J(r_{ij})S_iS_j\big)\right) \\ &= \frac{1}{Z}\prod_{\langle ij\rangle} e^{-v(r_{ij})} e^{K(r_{ij})S_iS_j}, \end{aligned} \tag{2.118}$$

where $\beta = 1/k_B T$, Z is the partition function, $K(r_{ij}) = \beta J(r_{ij})$ and $v(r_{ij}) = \beta V(r_{ij})$. For the second factor in the product we can differentiate the cases

$$\exp\big(K(r_{ij})S_iS_j\big) = \begin{cases} e^{K(r_{ij})}: & S_i = S_j \\ e^{-K(r_{ij})}: & S_i \neq S_j \end{cases}. \tag{2.119}$$

Considering this, we can rewrite the probability density using Kronecker deltas:

$$\begin{aligned} P(\{S\},\{\mathbf{r}\}) &= \frac{1}{Z}\prod_{\langle ij\rangle} \mathrm{e}^{-\nu(r_{ij})}\Big[\delta_{S_iS_j}\mathrm{e}^{K(r_{ij})} + \Big(1-\delta_{S_iS_j}\Big)\mathrm{e}^{-K(r_{ij})}\Big] \\ &= \frac{1}{Z}\prod_{\langle ij\rangle} \mathrm{e}^{-\nu(r_{ij})+K(r_{ij})}\Big[\mathrm{e}^{-2K(r_{ij})} + \Big(1-\mathrm{e}^{-2K(r_{ij})}\Big)\delta_{S_iS_j}\Big]. \end{aligned} \tag{2.120}$$

With the choice

$$p_{ij} = 1-\mathrm{e}^{-2K(r_{ij})} \tag{2.121}$$

this becomes

$$\begin{aligned} P(\{S\},\{\mathbf{r}\}) &= \frac{1}{Z}\prod_{\langle ij\rangle} \mathrm{e}^{-\nu(r_{ij})+K(r_{ij})}\prod_{\langle ij\rangle}\Big[(1-p_{ij})+p_{ij}\delta_{S_iS_j}\Big] \\ &= \frac{1}{Z'(\{\mathbf{r}\})}\prod_{\langle ij\rangle}\Big[(1-p_{ij})+p_{ij}\delta_{S_iS_j}\Big]. \end{aligned} \tag{2.122}$$

In the last step, a purely r-dependent factor has been absorbed in the partition function. This is possible, since spin and space configuration are updated independently and the configuration $\{\mathbf{r}\}$ is constant throughout one SW step. At this point, the probability density has a very similar form as for the standard Ising model.

A SW Monte Carlo move can be divided into two steps:

1. We start with a spin configuration. Neighboring spins S_i, S_j are connected by a bond with probability p_{ij}, if they are equal. The spin configuration is thereby transformed to a cluster configuration. A cluster can consist of multiple spins interconnected by bonds or it can be a single spin.

2. Each cluster is assigned a new spin value with probability $1/2$. The cluster configuration is then transformed back to a spin configuration.

In order to form the cluster configuration, neighboring spins S_i, S_j are connected with probability p_{ij}, if they are equal and with probability 0, if they are different. If two spins S_i, S_j are connected by a bond, we will denote that by $b_{ij} = 1$, otherwise by $b_{ij} = 0$. The conditional probability for a bond b_{ij} given a spin configuration $\{S\}$ is thus given by

$$P(n_{ij}|\{S\}) = \Big((1-p_{ij})\delta_{b_{ij}0} + p_{ij}\delta_{b_{ij}1}\Big)\delta_{S_iS_j} + (1-\delta_{S_iS_j})\delta_{b_{ij}0}. \tag{2.123}$$

Since all bonds can be treated as independent of each other, this can be extended to the whole configuration $\{b\}$, by taking the product

$$\begin{aligned} P(\{b\}|\{S\}) &= \prod_{\langle ij\rangle} P(b_{ij}|\{S\}) \\ &= \prod_{\langle ij\rangle}\Big[\delta_{b_{ij}0}(1-p_{ij}\delta_{S_iS_j}) + p_{ij}\delta_{b_{ij}1}\delta_{S_iS_j}\Big]. \end{aligned} \tag{2.124}$$

By applying Bayes' theorem, we find for the distribution of bonds, that

$$\begin{aligned} P(\{b\}) &= \sum_{\{S\}} P(\{b\},\{S\}) = \sum_{\{S\}} P(\{b\}|\{S\})P(\{S\}) \\ &= \frac{1}{Z'(\{\mathbf{r}\})} \sum_{\{S\}} \prod_{\langle ij\rangle} \Big(\Big[\delta_{b_{ij}0}(1-p_{ij}\delta_{S_iS_j}) + p_{ij}\delta_{b_{ij}1}\delta_{S_iS_j} \Big] \Big[(1-p_{ij}) + p_{ij}\delta_{S_iS_j} \Big] \Big) \\ &= \frac{1}{Z'(\{\mathbf{r}\})} \sum_{\{S\}} \prod_{\langle ij\rangle} \Big[(1-p_{ij})\delta_{b_{ij}0} + p_{ij}\delta_{b_{ij}1}\delta_{S_iS_j} \Big] \\ &= \frac{1}{Z'(\{\mathbf{r}\})} \sum_{\{S\}} \left[\prod_{\langle ij\rangle, b_{ij}=1} p_{ij}\delta_{S_iS_j} \prod_{\langle ij\rangle, b_{ij}=0} (1-p_{ij}) \right]. \end{aligned} \tag{2.125}$$

The sum can be evaluated by splitting it up into sums over individual clusters. The Kronecker delta $\delta_{S_iS_j}$ ensures, that within one cluster all spins are equal. Since for every cluster there are two possible spin orientations, this leads to a factor 2^{n_c}, if there are n_c clusters in the system:

$$P(\{b\}) = \frac{2^{n_c}}{Z'(\{\mathbf{r}\})} \left[\prod_{\langle ij\rangle, b_{ij}=1} p_{ij} \prod_{\langle ij\rangle, b_{ij}=0} (1-p_{ij}) \right]. \tag{2.126}$$

From Eq. (2.125) we see, that

$$P(\{b\},\{S\}) = \frac{1}{Z'(\{\mathbf{r}\})} \left[\prod_{\langle ij\rangle, b_{ij}=1} p_{ij}\delta_{S_iS_j} \prod_{\langle ij\rangle, b_{ij}=0} (1-p_{ij}) \right] \tag{2.127}$$

and therefore

$$P(\{S\}|\{b\}) = \frac{P(\{S\},\{b\})}{P(\{b\})} = 2^{-n_c} \prod_{\langle ij\rangle, b_{ij}=1} \delta_{S_iS_j}, \tag{2.128}$$

where the product of Kronecker deltas again ensures consistency. This can be interpreted as the second step, where all clusters are assigned a random spin with probability $1/2$.

We can use the above findings to verify, that the described algorithm satisfies the detailed balance condition and thus is a valid simulation method. For this purpose, we take the master equation

$$Q(\{S'\}, t+1) = \sum_{\{b\}} P(\{S'\}|\{b\}) \sum_{\{S\}} P(\{b\}|\{S\}) Q(\{S\}, t). \tag{2.129}$$

By using $Q(\{S\}, t) = P(\{S\})$ as input, which is Boltzmann distributed by definition, we find that

$$Q(\{S'\}, t+1) = P(\{S'\}). \tag{2.130}$$

This shows, that the Boltzmann distribution is stationary with respect to the Markov chain and detailed balance is indeed satisfied.

Hoshen-Kopelman algorithm

During the simulation, we need to assign to each particle the label of the cluster to which they belong. In practice, the recursive labeling of the clusters is rather costly in terms of computing time. A much more efficient way of cluster labeling offers the *Hoshen-Kopelman algorithm* [23], which is a special case of the union-find algorithm.

The basic idea is as follows: For every particle i, there is a particle label π_i, denoting the number of the cluster to which a particle belongs. Additionally, there is a list of cluster labels γ_j. A positive value of γ_j represents the number of particles in the cluster with index j, i.e. cluster j consists of γ_j particles. A negative value $-k,\ k>0$ of γ_j indicates, that cluster j is actually part of another cluster with index k.

We start by setting $\pi_i = i$ and $\gamma_i = 1$ for all i and then scan the lattice systematically. For each particle, the spins of half the next neighbors are checked and a bond is formed with probability p, if they are equal. If for the current particle no bonds are formed, the particle remains in its current one-particle cluster. Otherwise, if there are one or more bonds formed, the particle will be attached to the cluster with the lowest index. All other clusters will then be set to link to that cluster transferring their particle numbers. This way, if two clusters j and k become connected by a bond, one only has to set $\gamma_j = \gamma_j + \gamma_k$ and $\gamma_k = -j$, instead of relabeling the whole cluster in a second scan of the lattice.

Furthermore, the cluster sizes themselves carry some information. For example the susceptibility χ can be computed by the second moment of the cluster size distribution [24].

2.7 Implementation

In this section, the implementation of the model is discussed. The simulated model differs from the effective Hamiltonian derived in Sec. 2.2 by the fact, that the microscopic elastic degrees of freedom are explicitly taken into account. In theory they can be eliminated under the assumption, that a linear theory of elasticity is adequate.

First of all it should be noted, that the simple cubic lattice is no good choice for the simulation, because it is not shear-stable. The lattice could be sheared to zero volume without any cost of energy. For shear stability to be given, the coordination number $\mathscr{Z}$ must exceed twice the spacial dimension d. This is a special case of Maxwell's rule [25]. One lattice satisfying this rule is the face-centered cubic (fcc) lattice, where $\mathscr{Z} = 12$ (see Fig. 2.11). Also the fcc lattice has cubic

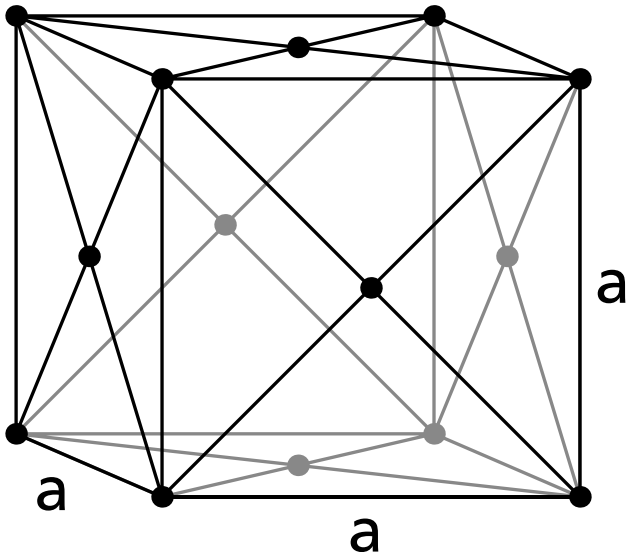

Figure 2.11: Illustration of the face-centered cubic lattice.

symmetry and hence is a good candidate for the implementation of the present model. We chose the lattice constant to be $a = \sqrt{2}$ so that the next neighbor distance is unity. We can then express the physical length of the box $\tilde{L}$ as

$$\tilde{L} = \frac{L}{\sqrt{2}}, \tag{2.131}$$

where the counting length L is a simulation parameter and must be an even integer. The number of particles N in a box of size L is then given by

$$N = \frac{L^3}{2}. \tag{2.132}$$

This is, because there are four particles per unit cell and $(L/2)^3$ cells in total.

In contrast to the effective Hamiltonian described in section 2.2, a more elementary Hamiltonian is used for the actual simulation. Here the elastic degrees of freedom are explicitly included with a harmonic potential

$$U_{\mathrm{el}}(\{\mathbf{r}\}) = \frac{K}{2} \sum_{\langle ij \rangle} (r_{ij} - l_0)^2, \tag{2.133}$$

where K is the spring constant, $r_{ij} = \left|\mathbf{r}_i - \mathbf{r}_j\right|$ and l_0 is the elastic equilibrium distance. The magnetic energy is similar to that of the rigid Ising model:

$$U_{\mathrm{mag}}(\{S\}) = -\sum_{\langle ij\rangle} J(r_{ij}) S_i S_j. \tag{2.134}$$

Here a distance dependent coupling constant $J(r_{ij})$ has been introduced. It is reasonable to assume, that the magnetic interaction decreases, as the spins move apart. One natural choice to model this behavior is an exponential decay

$$J(r_{ij}) = J_0 \exp\bigl(-\kappa(r_{ij} - l_0)\bigr), \tag{2.135}$$

with decay constant κ and a coupling strength $J_0 > 0$ for ferromagnetic behavior. We choose our unit system such that $l_0 = J_0 = k_{\mathrm{B}} = 1$. With this, the simulated Hamiltonian is given by

$$\mathscr{H}(\{\mathbf{r}\},\{S\}) = \frac{K}{2}\sum_{\langle ij\rangle}(r_{ij}-1)^2 - \sum_{\langle ij\rangle}\exp\bigl(-\kappa(r_{ij}-1)\bigr) S_i S_j. \tag{2.136}$$

The quantities of interest are the magnetization per particle

$$m = \frac{1}{N}\sum_{i=1}^{N} S_i \tag{2.137}$$

and the internal energy per particle

$$u = \frac{1}{N}\mathscr{H}(\{\mathbf{r}\},\{S\}). \tag{2.138}$$

At the beginning of this work, an initial program was supplied by B. Dünweg. The program relies on the Metropolis algorithm in order to update the magnetic as well as the elastic degrees of freedom in one composite step.

In each step, the lattice is scanned particle by particle. The spin of each particle is flipped with probability $1/2$. Furthermore, each of the particles coordinates r_i are shifted by a random value $-\delta \le \Delta r_j \le \delta,\ j = 1,\ldots,d$. The parameter δ is called maximum trial move and is a parameter of the simulation. In order to decide, whether the manipulation is accepted, the energy difference $\Delta E_i = E_i(t+1) - E_i(t),\ i = 1,\ldots,N$ is computed for each particle. If $\Delta E_i \le 0$, the move is accepted. Otherwise, the move will only be accepted with probability $\exp(-\Delta E_i/(k_{\mathrm{B}}T))$. This can easily be realized by generating a random number $0 \le \rho \le 1$ and only accepting the move if $\rho < \exp(-\Delta E_i/(k_{\mathrm{B}}T))$.

For a more detailed description of the Metropolis algorithm see e.g. [26]. One limitation of the Metropolis algorithm is the slow spin dynamic, especially near and below the critical point. This problem was avoided in this work by using the Swendsen-Wang cluster algorithm, which is described in detail in Sec. 2.6. For this purpose, magnetic and elastic degrees of freedom are updated independently.

Estimation of the optimal trial move

The value of the maximum trial move must be chosen reasonably in order to obtain a good acceptance rate, which is neither too high nor too low[4]. For this purpose we will roughly estimate the mean amplitude of the elastic fluctuations.

Consider a single particle in an elastic potential generated by $\mathscr{Z}$ nearest neighbors fixed in a lattice with cubic symmetry. For this purpose, we take the magnetic interaction to be constant. For a centered particle let $\mathbf{n}_i$, $i = 1, \ldots \mathscr{Z}$, $|\mathbf{n}_i| = l$ for all i, be the vectors pointing to the nearest neighbors. In case of cubic lattice symmetry, for each i there is exactly one $j \neq i$ s.t.

$$\mathbf{n}_i + \mathbf{n}_j = 0. \tag{2.139}$$

The elastic potential is given by

$$\begin{aligned} U_{\mathrm{el}}(r) =& \frac{K}{2} \sum_{i=1}^{\mathscr{Z}} (\mathbf{r} - \mathbf{n}_i)^2 \\ =& \frac{K}{2} \left[\mathscr{Z} r^2 + \mathscr{Z} l^2 - 2\mathbf{r} \left(\sum_{i=1}^{\mathscr{Z}} \mathbf{n}_i \right) \right] \\ =& \frac{\mathscr{Z} K}{2} (r^2 + l^2). \end{aligned} \tag{2.140}$$

The probability density of finding the particle at particular $\mathbf{r}$ can thus be written as

$$\begin{aligned} P(r) &\propto \exp(-\beta U_{\mathrm{el}}(r)) \\ &\propto \exp\left(-\mathscr{Z} \beta K r^2 / 2\right). \end{aligned} \tag{2.141}$$

The mean amplitude of the elastic fluctuations is then found by integrating

$$\begin{aligned} \sqrt{\langle r^2 \rangle} =& \left(\frac{\int \mathrm{d}^3\mathbf{r}\, r^2 \exp\left(-\mathscr{Z} \beta K r^2 / 2\right)}{\int \mathrm{d}^3\mathbf{r} \exp(-\mathscr{Z} \beta K r^2 / 2)} \right)^{1/2} \\ =& \left(\frac{\int_{-\infty}^{\infty} \mathrm{d}r\, r^4 \exp\left(-\mathscr{Z} \beta K r^2 / 2\right)}{\int_{-\infty}^{\infty} \mathrm{d}r\, r^2 \exp(-\mathscr{Z} \beta K r^2 / 2)} \right)^{1/2} \\ =& \sqrt{\frac{3}{\mathscr{Z} \beta K}}, \end{aligned} \tag{2.142}$$

which gives us a rough estimate for the optimal trial move to use in the simulation[5].

[4] A reasonable acceptance rate is around 0.5. This means that on average every second move is accepted.

[5] The same result can be obtained by adding a constant to the right hand side of Eq. (2.140) such that $U_{\mathrm{el}}(0) = 0$, and solving $U_{\mathrm{el}}(r) = 3k_{\mathrm{B}}T/2$ for r.

3 Evaluation

In this chapter, the results of the simulations are presented. The model as described in Sec. 2.7 has been simulated with *periodic boundary conditions* (i.e. constant volume) at several different linear system sizes L and temperatures T.

In Section 3.1, the simulation setup is described. The equilibration process is discussed and some basic dynamics are illustrated by using the example of correlation functions.

In Section 3.2, the parameters $\kappa = 1$ and $K = 3$ were used. We will from here on refer to this as *parameter set one*. The observables of interest have been reweighted with the multi histogram method described in Sec. 2.4. Then, the finite-size scaling methods as outlined in Sec. 2.3 were applied in order to determine the critical exponents of the system.

In Section 3.3, the magneto-elastic coupling was emphasized by setting $\kappa = 3$ and $K = 1$ (henceforth referred to as *parameter set two*). The basic structural properties of the ground state are discussed. Also some basic observations of the magnetic properties for $T > 0$ are made.

Finally, the work is summarized and an outlook on possible future work is given.

3.1 Basic Characteristics of the System

At the very beginning of the simulation, the fcc-lattice is set up. Coordinates and a set of next neighbors are assigned to every particle. This set of neighbors remains the same throughout the simulation. Since each particle only interacts with its next neighbors, this means that for high temperatures, the interaction partners of a particle must not necessarily be the particles which are physically closest.

In the next step, the lattice is scaled such that the total energy of the system at $T = 0$ is minimal. In this case we can set all spins $S_i = 1$ and need to minimize the bond energy

$$u_{\text{bond}}(r) = \frac{K}{2}(r-1)^2 - \exp(-\kappa(r-1)). \tag{3.1}$$

This, however, is only practical for $K > \kappa \exp(\kappa)$, since otherwise the magnetic interactions exceed the elastic ones and u_{bond} is minimal for $r = 0$ (See Fig. 3.1). While a configuration

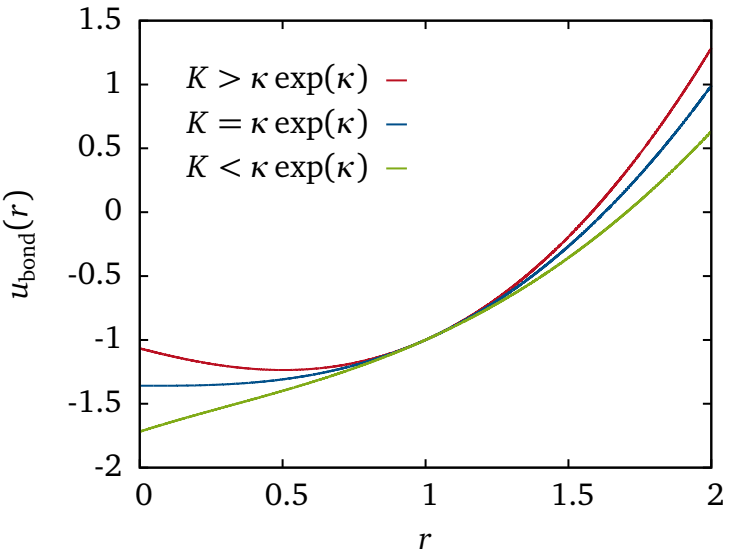

Figure 3.1: Bond potential Eq. (3.1) for different parameters κ and K.

where $r_{ij} = 0$ for all i, j, can certainly be the ground state for a system with free boundary conditions, this cannot be true for periodic boundary conditions. In this case, a state where all particles are centered in one point would imply strongly overstretched elastic bonds (For more details concerning the ground state see Sec. 3.3.). For this reason, the lattice will be set up such that $r = 1$ for all bonds in the case $K \leq \kappa \exp(\kappa)$, minimizing only the elastic energy, not the magnetic.

The two most important quantities being evaluated during the simulation are the internal energy per particle

$$u = \frac{\mathcal{H}}{N} = \frac{1}{N} \sum_{\langle ij \rangle} \left(\frac{K}{2}(r_{ij} - 1)^2 - S_i S_j \exp\big(-\kappa(r_{ij} - 1)\big) \right) \tag{3.2}$$

and the magnetization

$$m = \langle S \rangle = \frac{1}{N} \sum_i S_i. \tag{3.3}$$

At finite temperature, the initial configuration has to adapt to the fluctuations of the spins and it takes a number of Monte Carlo steps until the system reaches equilibrium, as can be seen in Fig. 3.2. There is a steep rise in internal energy (transient) in the first few steps corresponding

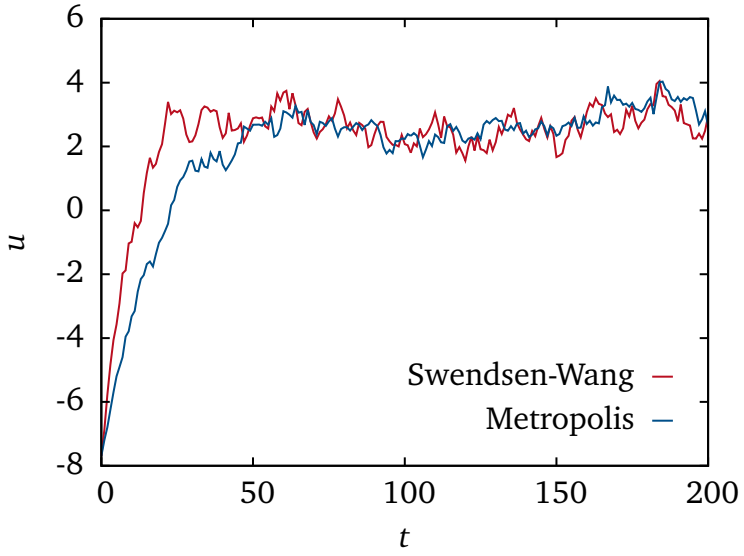

Figure 3.2: Time series of the internal energy u for $L = 10$, $T = 6.7$, $\kappa = 1$ and $K = 3$. The system needs about 50 steps to reach equilibrium. With the Swendsen-Wang algorithm equilibration is slightly faster than with the Metropolis algorithm.

to the heating of the system. Because of the faster spin dynamics, the Swendsen-Wang algorithm is able to equilibrate the system quite a bit faster. While for small system sizes and moderate temperatures the equilibration time might be rather short, this effect amplifies rapidly with increasing size and decreasing temperature. Equilibration time can reach several thousand steps for big systems. The corresponding points must of course be omitted, when evaluating the time series.

The effect also becomes apparent when considering the correlation function (see Fig. 3.3). For this purpose, we will use a biased estimator for the correlation function [18]

$$c_t(x) = \frac{1}{N-t}\sum_{i=1}^{N-1}(x_i - \bar{x})(x_{i+t} - \bar{x}), \tag{3.4}$$

which will be sufficient to see the qualitative behavior. From Fig. 3.3b it is apparent, that the Swendsen-Wang algorithm has a considerably smaller correlation time than the Metropolis algorithm. The reason for this is the faster spin dynamics of the Swendsen-Wang algorithm, which can be seen from Fig. 3.3a. While for the Metropolis algorithm the correlation function of the spin drops down continuously, the correlation function of the Swendsen-Wang algorithm instantly drops below the limit of precision. This in turn allows for the internal energy to relax faster (Fig. 3.3b).

In order to improve the performance of the simulation even further, one should focus on the elastic dynamics next. This could be improved by considering algorithms like the Fourier Monte Carlo algorithm [27, 28] or Multigrid Monte Carlo methods [29, 30].

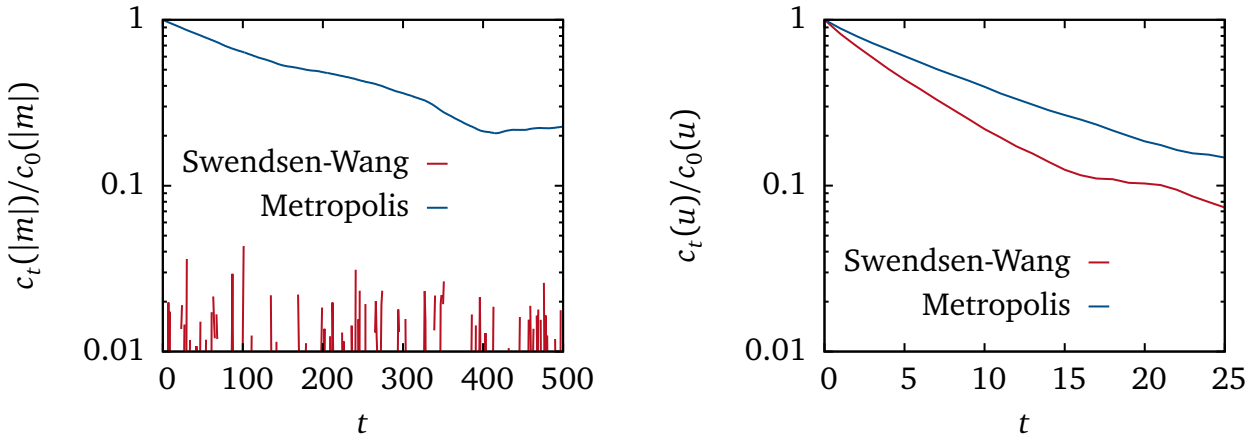

(a) Correlation function of the magnetization.

(b) Correlation function of the internal energy.

Figure 3.3: Correlation functions for $L = 100,\ T = 7.14,\ \kappa = 1$ and $K = 3$. Comparison between Swendsen-Wang and Metropolis algorithm.

3.2 Determination of the Critical Exponents

For the determination of the critical exponents, finite-size scaling methods as outlined in Sec. 2.3 have been used in the spirit of Ferrenberg and Landau in [31]. The simulated systems with their respective parameters are listed in Tab. 3.1. Since periodic boundary conditions (2.42) were applied, we would expect a second order phase transition with Fisher renormalized exponents from the theory in Sec. 2.2.

The first step was to determine the critical exponent of the correlation length ν. For this, the scaling behavior with the linear system size L of the maximum slopes

$$\left.\frac{\partial \log(\langle |m|^n \rangle)}{\partial B}\right|_{\max} \propto L^{1/\nu}, \tag{3.5}$$

has been utilized. Here we define $B = 1/k_B T$, in order to avoid confusion with the critical exponent β. The Binder cumulant U [32] is defined by the ratio of moments

$$U = 1 - \frac{\langle m^4 \rangle}{3\langle m^2 \rangle^2}. \tag{3.6}$$

Its maximum derivative exhibits the same scaling behavior as the maximum logarithmic derivative of the magnetic moments:

$$\left.\frac{\partial U}{\partial B}\right|_{\max} \propto L^{1/\nu}. \tag{3.7}$$

The above derivatives can be computed with the formula

$$\frac{\partial \langle O \rangle}{\partial B} = \langle O \rangle \langle E \rangle - \langle OE \rangle, \tag{3.8}$$

which is easily obtained by taking the derivative of the Boltzmann mean value

$$\langle O \rangle = \frac{\int \mathrm{d}\Gamma\, O(\Gamma) \exp(-BE(\Gamma))}{\int \mathrm{d}\Gamma \exp(-BE(\Gamma))}. \tag{3.9}$$

For the derivative of the cumulant this gives us then

$$\frac{\partial U}{\partial B} = \frac{1}{3}\frac{\langle m^4 \rangle}{\langle m^2 \rangle^2}\left(\langle E \rangle + 2\frac{\langle m^4 E \rangle}{\langle m^4 \rangle} - \frac{\langle m^2 E \rangle}{\langle m^2 \rangle} \right). \tag{3.10}$$

The locations of the maximal slopes were determined by reweighting the above derivatives at different temperatures. For this purpose a temperature interval $\Delta T = T_{\max} - T_0$ was divided into n subintervals. The derivatives were then reweighted at temperatures $T_i = T_0 + i\Delta T/(n-1)$, $i = 0, \ldots, n-1$. This produced some point T_j, at which the derivative is maximal. The same procedure was then repeated iteratively with $T_0' = T_{j-1}$ and $T_{\max}' = T_{j+1}$ until the location of the peak was found with satisfactory precision. For this to work, one has to make sure, that sufficient data is available within the reweighting interval. Otherwise there might be more

L	κ	K	T	$t_{\max}/10^5$	δ
12	1	3	6.80	11	0.433
	1	3	6.85	11	0.435
	1	3	6.90	11	0.437
	1	3	6.95	11	0.439
	1	3	7.00	11	0.440
	1	3	7.04	11	0.441
	1	3	7.10	11	0.443
	1	3	7.14	11	0.444
	1	3	7.20	11	0.447
18	1	3	6.80	11	0.433
	1	3	6.85	11	0.435
	1	3	6.90	11	0.437
	1	3	6.95	11	0.439
	1	3	7.00	11	0.440
	1	3	7.04	11	0.441
	1	3	7.10	11	0.443
	1	3	7.14	11	0.444
	1	3	7.20	11	0.447
26	1	3	6.80	11	0.433
	1	3	6.85	11	0.435
	1	3	6.90	11	0.437
	1	3	6.95	11	0.439
	1	3	7.00	11	0.440
	1	3	7.04	11	0.441
	1	3	7.10	11	0.443
	1	3	7.14	11	0.444
	1	3	7.20	11	0.447
38	1	3	6.80	11	0.433
	1	3	6.85	11	0.435
	1	3	6.90	11	0.437
	1	3	6.95	11	0.439
	1	3	7.00	11	0.440
	1	3	7.04	11	0.441
	1	3	7.10	11	0.443
	1	3	7.14	11	0.444
	1	3	7.20	11	0.447
58	1	3	6.95	11	0.439
	1	3	7.00	11	0.440
	1	3	7.05	11	0.441
	1	3	7.10	11	0.443
86	1	3	6.95	11	0.439
	1	3	7.00	11	0.440
	1	3	7.05	11	0.441
	1	3	7.14	11	0.444

Table 3.1: Simulation parameters: L is the counting length, κ is the constant of magnetic interaction, K is the spring constant, T is the temperature, n is the number of Monte Carlo steps and δ is the maximum trial move. All simulations have been performed with periodic boundary conditions and the ratio of elastic (Metropolis) to magnetic (Swendsen-Wang) updates is 1:1. Before simulation, the lattice is scaled so that Eq. 3.1 is minimal. This results in a next neighbor distance in the undisturbed lattice of about 0.3809.

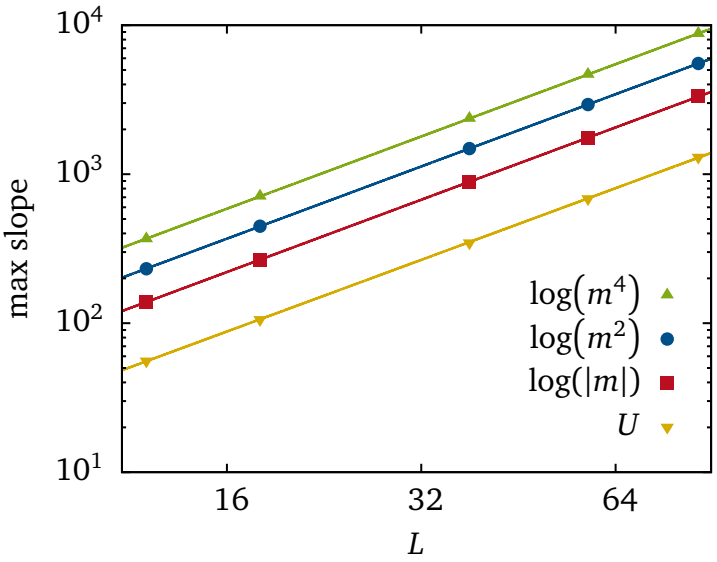

Figure 3.4: Double logarithmic plot of the maximum logarithmic slope of different magnetic moments m^n as well as the maximum slope of the Binder cumulant U vs. the linear system size L.

than one peak due to statistical errors. Alternatively, one could reweight the data in a suitable temperature interval and determine the peaks by fitting a parabola.

A double-logarithmic plot of Eq. (3.5) and (3.7) vs. L should produce straight lines with slope $1/\nu$. This was done in Fig. 3.4, yielding an exponent of

$$\nu = 0.62210(58).$$

Note, that the error values in this section are merely the asymptotic standard errors from the fitting procedure, and not the real statistical errors. The real errors are expected to be slightly bigger.

The value above of ν was then used to determine the critical temperature T_c. As we know from Sec. 2.3, in finite systems

$$T_c(L) - T_c \propto L^{-1/\nu} \tag{3.11}$$

holds. This means, that $T_c(L)$ converges to the real critical temperature as $L \to \infty$. The temperatures, at which the slopes of $\log(|m^n|)$ and U are steepest were taken as estimators for $T_c(L)$. Also the temperatures, at which the specific heat C as defined in Eq. (2.88) and the susceptibility χ are maximal were used. From here on the symbol χ will always denote the finite lattice susceptibility as defined in Eq. (2.83).

A plot of Eq. (2.90) vs. $L^{1/\nu}$ results in straight lines, that can be extrapolated to $L \to \infty$. This is shown in Fig. 3.5. The value obtained from C was not taken into account, since the peak of C is at much lower temperature as the actually simulated temperatures for almost all sizes. The reweighting is therefore expected to produce significant systematic errors. The linear extrapolation to $L^{-1/\nu}$ yielded a critical temperature of

$$T_c = 7.00850(41).$$

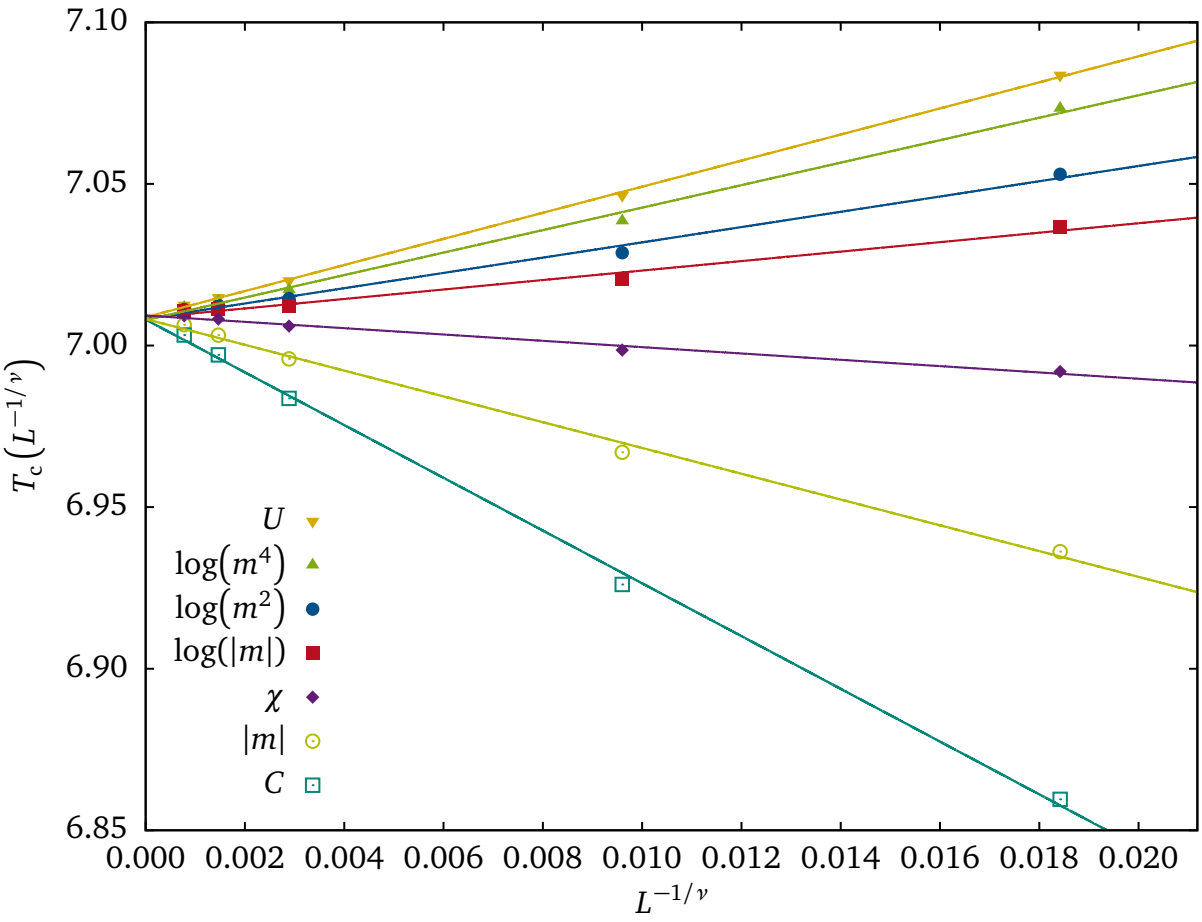

Figure 3.5: Plot of size dependent critical temperature T_c obtained from different variables.

In Sec. 2.3, the scaling behavior of $|m|$, χ and C was derived:

$$|m| \propto L^{-\beta/\nu}, \tag{3.12}$$

$$\chi \propto L^{\gamma/\nu}, \tag{3.13}$$

$$C \propto L^{\alpha/\nu}. \tag{3.14}$$

These above relations were used to determine the exponents α, β and γ. The observables were reweighted at the critical temperature determined earlier. The respective exponents were then taken from the slopes of a double logarithmic plot (see Fig. 3.6), yielding

$$\begin{aligned}\beta &= 0.2876(90),\\ \gamma &= 1.2499(26),\\ \alpha &= 0.1824(55).\end{aligned}$$

Since the value of α was obtained from the scaling of C, it is most likely afflicted with a

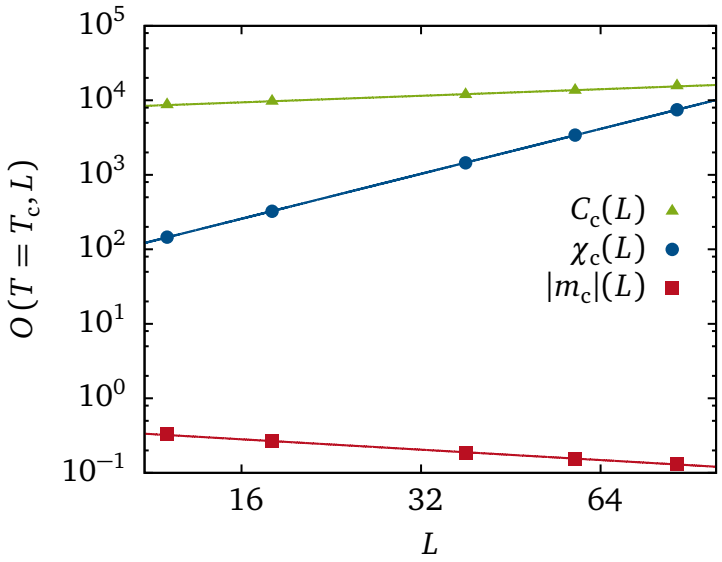

Figure 3.6: Scaling behavior of $|m|$, χ and C with L at criticality in a double logarithmic plot. The exponents β, γ and α were determined by the slopes.

significant error for the same reasons mentioned above.

In Table 3.2 the values of the critical exponents of the present are compared to the exponents of the standard Ising models and their Fisher renormalized value. It is clear, that despite the theoretical considerations in Sec. 2.2 there is *no evidence for Fisher renormalization* with the given parameters. In fact, the exponents found, are closer to the exponents of the regular Ising model, as they are to their Fisher renormalized counterparts. If we insert the exponents in the hyperscaling relation Eq. (2.80), we find that

$$\alpha + d\,\nu = 2.0487(58), \tag{3.15}$$

which deviates from the expected value of 2 by 3%.

It remains to identify the reasons, for which the theory described in Sec. 2.2 fails in the current case. One possibility is, that the simulation parameters κ and K were chosen in a way,

exponent	Ising	F-renormalized	present work
ν	0.6289(8)	0.7066(37)	0.622 10(58)
α	0.1100(45)	−0.1236(51)	0.1824(55)
β	0.3258(44)	0.3661(52)	0.2876(90)
γ	1.2390(71)	1.392(11)	1.2499(26)

Table 3.2: Critical exponents of the standard Ising model, their Fisher-renormalized value and the values found in the present work. The Ising values of β, ν and γ here determined by finite-size scaling analysis in [31]. The specific heat exponent α was computed with renormalization group theory methods in [33].

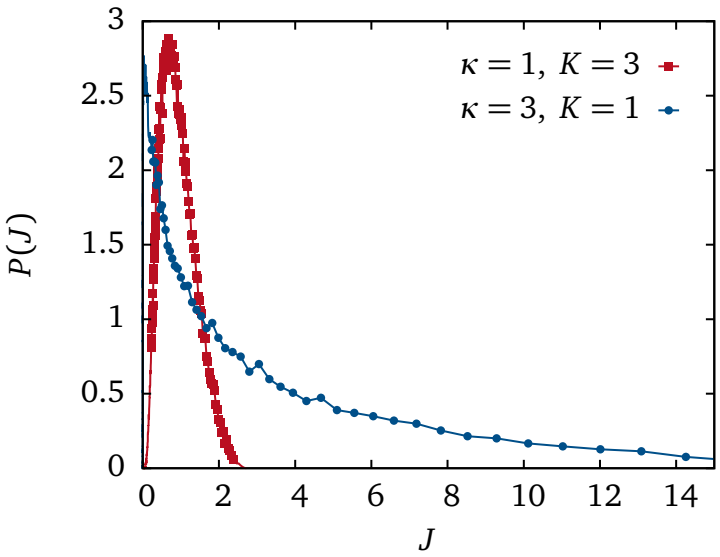

Figure 3.7: Plot of the histograms $P(J)$ for different parameter sets (κ, K) at temperature $T = 7.00$.

that results in negligible coupling between the elastic and magnetic degrees of freedom. For a reasonable coupling strength, one would expect the standard deviation of the probability density $P(J)$ to be of the order $k_B T$ for $T \approx T_c$. A plot of $P(J)$ for different parameters can be seen in Fig. 3.7. Since $k_B = 1$ in our unit system, we would need the width of $P(J)$ to be approximately seven. For our initial parameter set ($\kappa = 1$, $K = 3$), the width is about two, which might not be enough.

In order to strengthen the coupling, we can soften the springs by decreasing K and amplify the decay of magnetic interaction by increasing κ. For $\kappa = 3$ and $K = 1$, the distribution is already much broader[1] and might be a more promising choice for seeing the influences of elastic coupling. In the next section we will continue by examining the ground state for the second set of parameters.

[1] Although $T = 7.00$ must not necessarily be near T_c for this set of parameters.

3.3 Properties of the Ground State

In the following, the structural properties of the ground state will be discussed. By ground state we mean the state of lowest energy. This means, that we can assume that $T = 0$ and $S_i = 1$ for all i.

Here we consider the special case, where $K < \kappa \exp(\kappa)$, namely $\kappa = 3$ and $K = 1$. This means, that the bond potential

$$u_{\text{bond}}(r) = \frac{K}{2}(r-1)^2 - \exp(-\kappa(r-1)) \tag{3.16}$$

has its minimum at $r = 0$ (see Fig. 3.1). As a consequence, all particles want to contract into one point. This however, is prevented by the periodic boundary conditions. If all particles were located in one single point, there would be some strongly overstretched elastic bonds, reaching all the way over to a periodic image of the box.

The energy of such a state can be computed by counting the fraction of bonds, that are extending to a periodic image (periodic bonds), and the number of bonds lying entirely within the box (volume bonds). For the fcc lattice there are

$$n_{\text{bonds}} = \frac{\mathscr{Z}}{2} N = 3L^3 \tag{3.17}$$

bonds in total ($\mathscr{Z} = 12$ denoting the number of next neighbors in the fcc lattice). A number of $6L(L-1)$ bonds are connected to a neighbor in an adjacent box, that shares a face with the simulation box. This means, that the periodic box is displaced by $\tilde{L}$ in exactly one of the three spacial directions relative to the simulation box ($\tilde{L} = L/\sqrt{2}$ denoting the physical box length as defined in Sec. 2.7). Furthermore, there are $3L$ periodic bonds, where the corresponding periodic box is displaced by $\tilde{L}$ in two spacial directions, meaning, that the origins of both boxes are $\sqrt{2}\tilde{L}$ apart from each other. In the case of the fcc lattice, there are no bonds, for which the periodic box is displaced along all three of the spacial dimensions. This leaves us with a remainder of $3L^3 - 6L^2 + 3L$ volume bonds. Now we can compute the energy of the collapsed state with

$$\begin{aligned} E_{\text{collapsed}} =& \left(3L^3 - 6L^2 + 3L\right) u_{\text{bond}}(0) \\ &+ 6L(L-1) u_{\text{bond}}\left(\tilde{L}\right) \\ &+ 3L u_{\text{bond}}\left(\sqrt{2}\tilde{L}\right). \end{aligned} \tag{3.18}$$

Since the next neighbor distance is exactly unity in the undisturbed lattice, the energy of the perfect lattice state is given by

$$E_{\text{pl}} = -6N. \tag{3.19}$$

The energies of both those configurations are compared in Fig. 3.8. From the graph we see, that for $L < 37$ the collapsed state is energetically favored, as opposed to the perfect lattice. For $L > 37$ however, the perfect lattice offers lower energy. This means, that the collapsed state will certainly not be the ground state for $L > 37$. For smaller L however, the collapsed state could

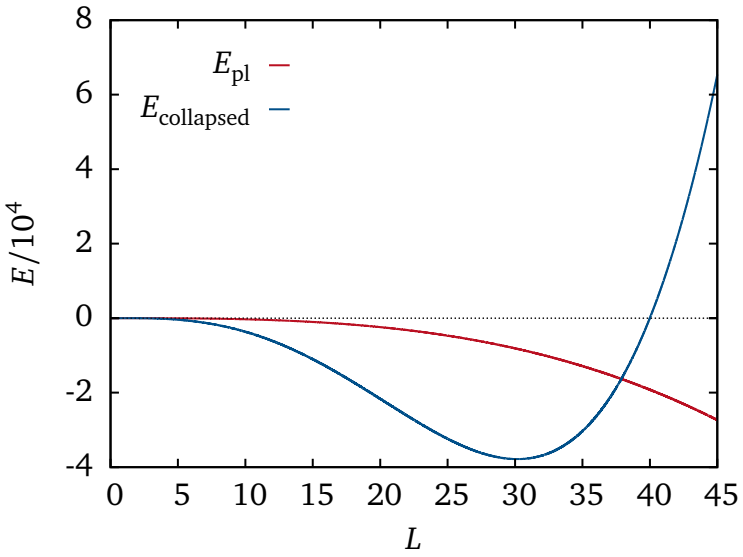

Figure 3.8: Energy of the collapsed state $E_{\mathrm{collapsed}}\left(\tilde{L}\right)$ in comparison with the energy of the perfect lattice $E_{\mathrm{pl}}(\tilde{L})$ vs. L for the three-dimensional system. All spins are equal to 1.

be the ground state. Simulation showed, that this is only the case for very small sizes ($L \lesssim 4$) and for intermediate sizes there are mixed configurations (see Sec. 3.3.2).

As it turns out, it is very hard to find the true ground state of the system in practice. The system gets easily trapped in a local minimum of the energy landscape. In order to escape from such a local minimum, the system would have to perform a collective change in configuration, which is very unlikely and would therefore require a lot of Metropolis steps.

In order to get some first insights into the general behavior of the system at $T = 0$, the one-dimensional case was considered first, before covering the three-dimensional case.

3.3.1 Ground State in One Dimension

In the one-dimensional case, we can make similar considerations in order to compute the energy. The system consists of L particles and is set up such, that the next neighbor distance is unity. This means, that L coincides with the physical length of the system.

We again differentiate between the perfect lattice and the collapsed state, where in the latter case, there is only one periodic bond and the remaining bonds are volume bonds. This yields for the collapsed state

$$E_{\mathrm{collapsed}} = (L-1)u_{\mathrm{bond}}(0) + u_{\mathrm{bond}}(L), \tag{3.20}$$

and for the perfect lattice

$$E_{\mathrm{pl}} = Lu_{\mathrm{bond}}(1) = -L. \tag{3.21}$$

Both energies are compared for different system sizes L in Fig. 3.9. It is evident, that for $L > 36$, the completely collapsed state cannot be the true ground state. In fact we will find, that the collapsed state is only the true ground state for very small L.

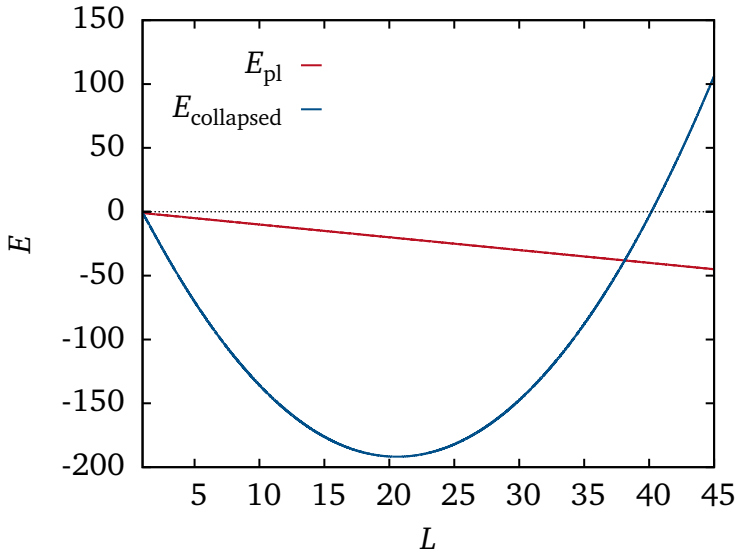

Figure 3.9: Energy of the collapsed state $E_{\text{collapsed}}(L)$ in comparison with the energy of the perfect lattice $E_{\text{pl}}(L)$ vs. L for the one-dimensional system. All spins are equal to 1.

The simulated annealing [34, 35, 36, 37] method was used, to find an approximation of the ground state. The method is inspired by the gentle cooling of alloys in order to remove any internal stresses. In order to do so in simulation, the following cooling schedule was implemented (see Fig. 3.10):

$$T(t) = T_0\left(\exp\left(-2\frac{t}{t_{\max}}\right)\left(1-\frac{t}{t_{\max}}\right)\left(1+\sin\left(2\pi n\frac{t}{t_{\max}}\right)\right)\right). \tag{3.22}$$

The first term produces an exponential decay of the temperature T over time t, while the second term ensures, that the temperature is indeed zero at the end of the simulation, where $t = t_{\max}$. The last term produces a periodical (n-times) reheating. This cooling schedule was chosen heuristically by trying several different schedules and choosing the most successful. As temperature is reduced, the maximum trial value δ has to be reduced accordingly. This was done automatically during simulation: Every time the acceptance rate fell below 0.3 δ was decreased by 10% and every time the acceptance rate exceeded 0.7 δ was increased by 10%. This is appropriate, since we are not interested in dynamic, but only structural properties. If needed, the whole procedure can be repeated, using the last configuration as new initial configuration and possibly with lower T_0, until a satisfactory outcome is reached.

The configurations resulting from this procedure, are systems of *multiple clusters*, where within a cluster the particle distance r is nearly zero (at least $r < 10^{-6}$). The configuration and bond-length histogram for $L = 22$ are plotted in Fig. 3.11. In order to illustrate the periodic boundary conditions, the configuration was mapped to a circle. From the bond-length histogram in Fig. 3.11b we see, that the four individual clusters almost have identical distance from each other (around 5.5). For symmetry reasons, we would expect the clusters to be actually equidistant and therefore expect 18 bonds with $r = 0$ and four bonds with $r = 22/5 = 5.5$. In fact, if the particles are constrained to four equidistant clusters, the ground state energy per particle can be further reduced from -14.1787 to -14.1836.

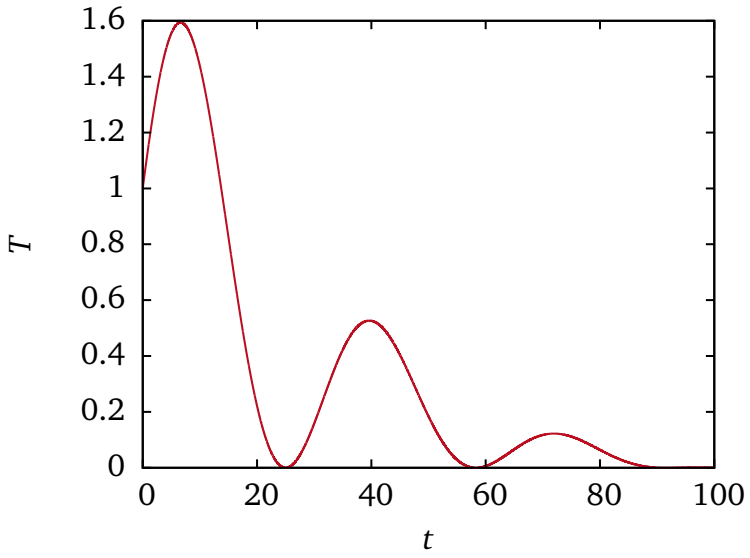

Figure 3.10: Cooling schedule with $T_0 = 1$, $t_{\max} = 100$ and $n = 3$.

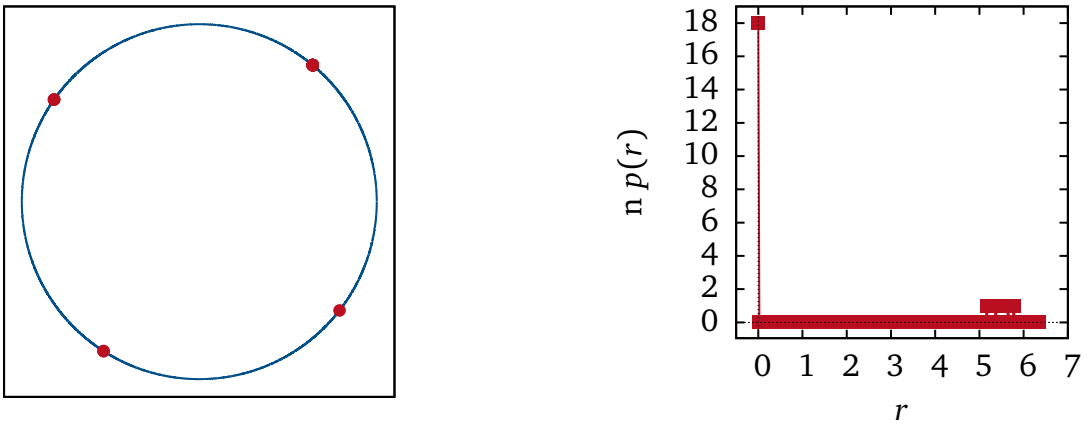

(a) Configuration

(b) Bond-length histogram

Figure 3.11: Ground state for $L = 22$. The results were obtained by simulated annealing with $T_0 = 40$, $n = 4$ and $t_{\max} = 10^7$.

The simulated annealing method as it was implemented here, was not sufficient to reach the absolute energy minimum, but gave a good first insight. Furthermore, the method can easily become stuck in configurations with a higher number of clusters, yielding even higher energies.

The number of clusters formed is dependent on the system size L; the larger the system, the more clusters there are. We will now evaluate the energy of such a n-cluster system. Assuming, that within one cluster the particle distance is exactly zero and that per cluster there is exactly one bond reaching over to the next cluster, we can write the energy as:

$$E(L,n) = n u_{\text{bond}}(L/n) + (L-n) u_{\text{bond}}(0). \tag{3.23}$$

The energy levels are degenerate in the sense that the distribution of particles among the clusters does not matter, as long as the connecting bonds have length L/n. Introducing the cluster distance $\zeta = L/n$, we can write the energy density as

$$\begin{aligned} \frac{E(\zeta)}{L} =& \frac{1}{\zeta} u_{\text{bond}}(\zeta) + \left(1 - \frac{1}{\zeta}\right) u_{\text{bond}}(0) \\ =& \frac{1}{\zeta}\left(\frac{K}{2}(\zeta-1)^2 - \exp(-\kappa(\zeta-1))\right) + \left(1-\frac{1}{\zeta}\right)\left(\frac{K}{2} - \exp(\kappa)\right). \end{aligned} \tag{3.24}$$

By numerical minimization we find, that this function has a global minimum at

$$\zeta_{\text{opt}} \approx 6.33807, \tag{3.25}$$

which corresponds to an energy density of about -14.2475. Since ζ is not really continuous, but a ratio of whole numbers, the system can only approximate this ideal value. However, we can minimize Eq. 3.24 for given L with respect to n, in order to find the optimum number of clusters. Some of the results are listed in Tab. 3.3. As can be seen from Fig. 3.12, the optimum value of ζ can be approximated better and better as system size is increased.

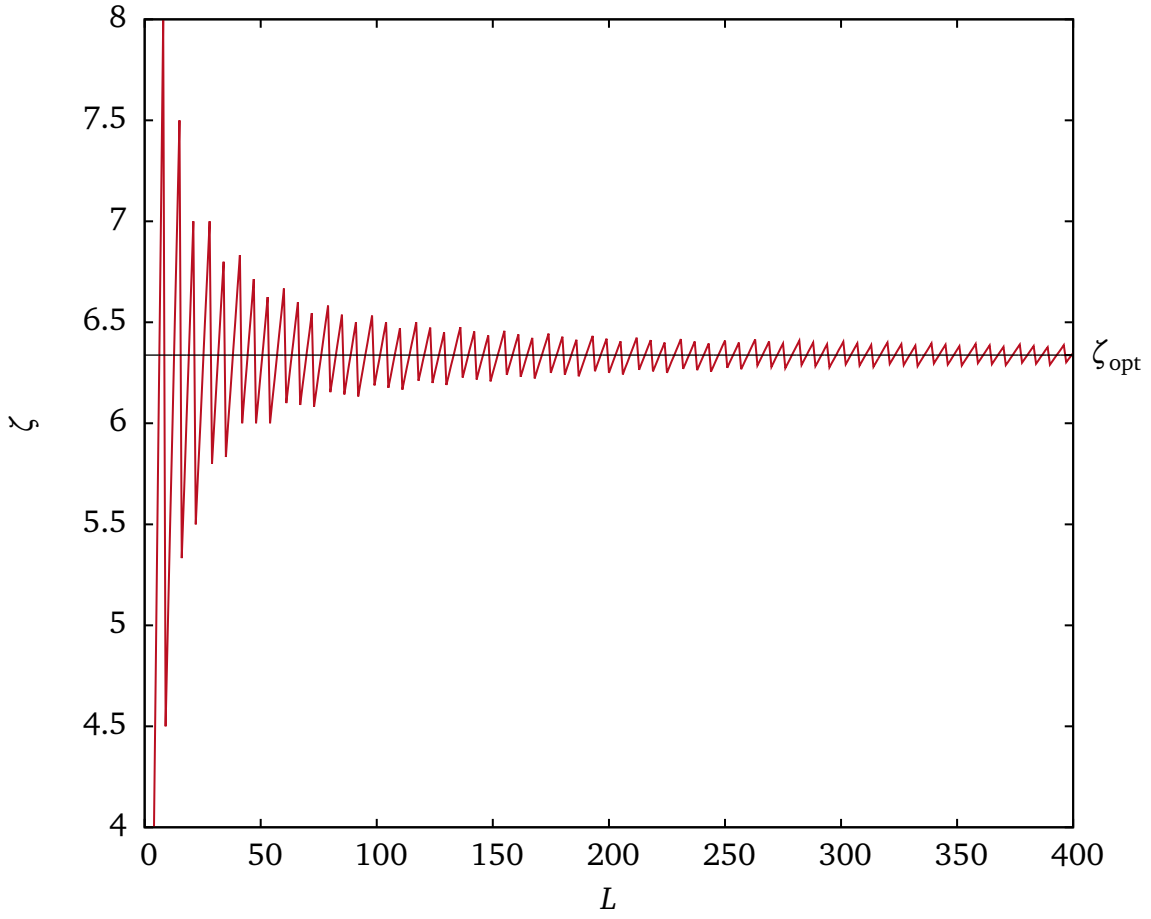

Figure 3.12: Closest possible approximation of ζ_{opt} vs. system-size L.

L	n	L/n	E	E/L
1	1	1.000	−1.0000	−1.000 000 0
9	2	4.500	−124.8488	−13.872 090 39
16	3	5.333	−226.4453	−14.152 832 51
22	4	5.500	−312.0397	−14.183 621 37
29	5	5.800	−412.4529	−14.222 513 41
35	6	5.833	−497.8972	−14.225 635 44
42	7	6.000	−597.9938	−14.237 947 49
48	8	6.000	−683.4215	−14.237 947 49
54	9	6.000	−768.8492	−14.237 947 49
61	10	6.100	−868.8124	−14.242 825 99
67	11	6.091	−954.2446	−14.242 456 95
73	12	6.083	−1039.676	−14.242 138 20
80	13	6.154	−1139.577	−14.244 714 13
86	14	6.143	−1225.016	−14.244 369 82
92	15	6.133	−1310.453	−14.244 054 49
100	16	6.250	−1424.685	−14.246 851 04
105	17	6.176	−1495.763	−14.245 357 58
111	18	6.167	−1581.205	−14.245 089 52
118	19	6.211	−1681.047	−14.246 161 91
124	20	6.200	−1766.496	−14.245 934 22
130	21	6.190	−1851.943	−14.245 712 12
137	22	6.227	−1951.769	−14.246 485 90
143	23	6.217	−2037.221	−14.246 300 39
149	24	6.208	−2122.671	−14.246 116 01
156	25	6.240	−2222.485	−14.246 700 90
161	25	6.440	−2293.713	−14.246 664 74
168	27	6.222	−2393.394	−14.246 393 12
175	28	6.250	−2493.199	−14.246 851 04
181	29	6.241	−2578.657	−14.246 722 59
187	30	6.233	−2664.113	−14.246 591 63
194	31	6.258	−2763.910	−14.246 960 13
200	32	6.250	−2849.370	−14.246 851 04
206	33	6.242	−2934.828	−14.246 738 81
213	34	6.265	−3034.620	−14.247 041 96
219	35	6.257	−3120.082	−14.246 948 20
225	36	6.250	−3205.541	−14.246 851 04
232	37	6.270	−3305.328	−14.247 104 97
238	38	6.263	−3390.792	−14.247 023 53
244	39	6.256	−3476.253	−14.246 938 62
251	40	6.275	−3576.036	−14.247 154 57
257	41	6.268	−3661.500	−14.247 083 16

Table 3.3: Expected number of clusters n for different system sizes L.

3.3.2 Ground State in Three Dimensions

In the three-dimensional case we conjecture, that the system behaves similar to the system in one dimension. Namely we assume, that there is the formation of multiple $r = 0$ clusters with a defined distance between each other. One obvious way to implement that, is to impose a superlattice on the system. This reduces the configuration space and therefore simplifies the detection of the ground state. In one Metropolis step, each particle is displaced to a random site of the superlattice, which is then either accepted or not, depending on the energy difference. As a consequence, particles can only occupy sites on said superlattice, while empty sites are allowed too.

A simple cubic (sc) as well as a face centered cubic (fcc) superstructure have been considered as superlattice. Since the simulated box has a linear length of L, the lattice constant of the superlattice a_s must be chosen such, that L/a_s is an integer[2]. This defines the counting length of the superlattice

$$L_s = L/a_s. \tag{3.26}$$

In the next step, the simulated annealing method from Sec. 3.3.1 was applied for various L_s, in order to find the specific superlattice, that allows for the lowest energy. The simulated systems and their energies are listed in Tab. 3.4. A plot of the resulting ground state energies for different system sizes is given in Fig. 3.13. Each simulation was run multiple times with

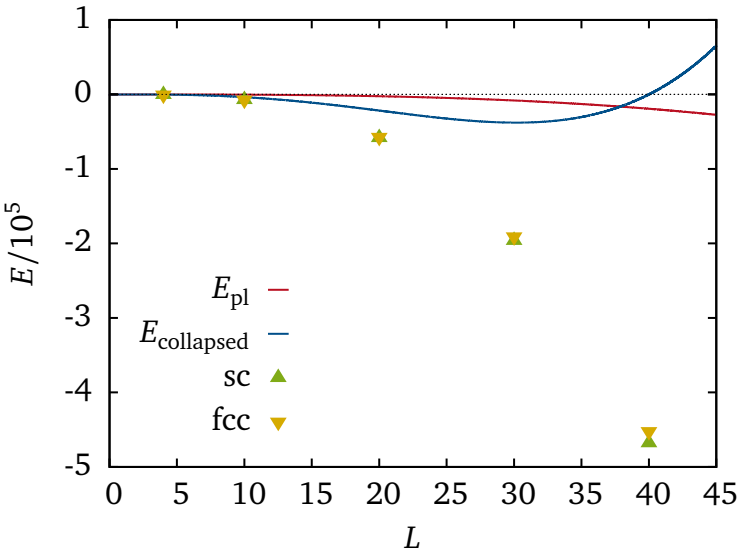

Figure 3.13: Energy of the collapsed state and the perfect lattice in comparison with the energy of the approximate ground with imposition of a superlattice. Significantly lower energies are reached by deviating from the before mentioned special cases. The convergence is nearly identical for both the sc and fcc superlattice.

simulated annealing for at least 10^5 steps, using the configuration of lowest energy from the

[2] If all possible lattice constants are considered, the set of sc configurations is actually equal to the set of fcc configurations. We can transfer a sc lattice with lattice constant a_s to a fcc lattice with lattice constant $2a_s$, by leaving suitable holes in the sc lattice and vice versa. It is nevertheless reasonable to examine both superstructures, since one of them might fit the true ground state configuration better.

L	L_s	E/L
4	1	−60.6620
	2	−60.6620
	3	−60.6620
	20	−60.6620
10	1	−72.8524
	2	−72.9046
	3	−73.0594
	4	−73.0384
	5	−73.0234
	6	−73.0549
	7	−73.0557
	8	−73.0430
20	1	−54.1241
	2	−72.8524
	3	−72.1833
	4	−67.8252
	5	−68.2839
30	1	−28.0153
	2	−65.3000
	3	−72.7223
	4	−72.6994
	5	−70.1355
40	1	0.0139
	2	−50.5594
	3	−68.3025
	4	−69.7187
	5	−73.1270
	6	−68.6745
	10	−48.3296

(a) sc superlattice

L	L_s	E/L
4	2	−60.6620
	4	−60.6620
	6	−60.6620
	8	−60.6620
10	2	−72.9046
	4	−72.8450
	6	−70.9516
	8	−62.2672
20	2	−57.5328
	4	−71.5171
	6	−67.4925
	8	−61.7311
30	2	−37.9208
	4	−67.8399
	6	−70.6801
	8	−67.1129
40	2	−15.0381
	4	−60.9168
	6	−69.8216
	8	−70.6495
	10	−68.9320
	12	−63.7280

(b) fcc superlattice

Table 3.4: Ground state energies for different system sizes L. For each size, several superlattices with counting length L_s have been examined, in order to find the structure of lowest energy. For $L = 4$, the collapsed state, where all particles are located in one point was found for both superlattices.

previous run as new initial condition. This was done, until there was no more significant reduction in internal energy. The overall lowest energy was then used as the approximate ground state energy. We find, that the energy of the true ground state is significantly lower than the energy of the collapsed state as well as the energy of the perfect lattice state. Also the energy per particle is nearly constant at

$$\frac{E}{N} \approx -72.2(10). \tag{3.27}$$

In this mean value, the cases $L = 4$, where there is only a single cluster, were not taken into account.

This confirms, that the energy is indeed an extensive variable as required by thermodynamics. Since our main concern is the critical behavior of the system and true phase transitions are inherent only to infinite systems, the behavior for $L \to \infty$ is most important. Keeping this in mind, $L = 40$ seems to be a good compromise between large system size and reasonable computing time.

At $L = 40$, the lowest energy was reached with clusters arranged in a cubic superlattice with counting length $L_s = 5$. Closer examination revealed, that the particles arrange in three mutually perpendicular planes. In the point common to all three planes, particle concentration is highest. This is shown in Fig. 3.14 (clusters with less than five particles in them were left out for clarity).

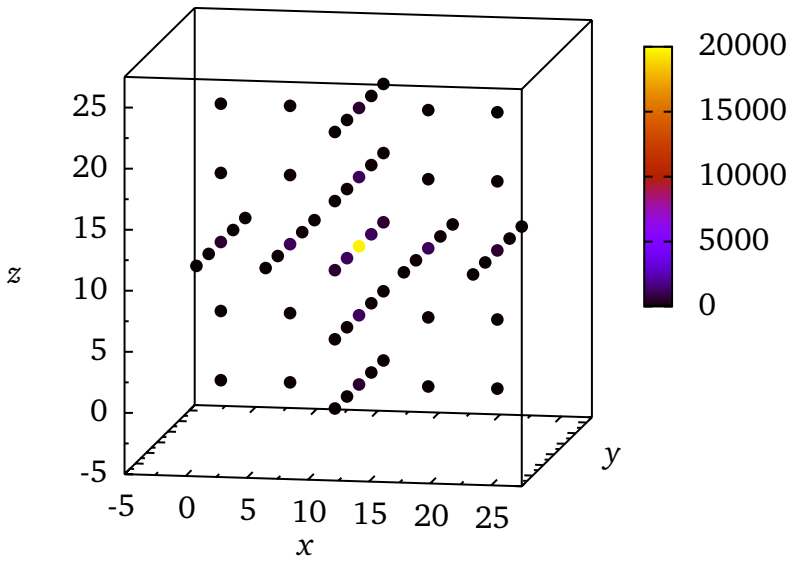

Figure 3.14: Ground state of the three-dimensional system, where a cubic superlattice with counting length $L_s = 5$ has been imposed. The particles arrange in three mutually perpendicular planes. Colors indicate the number of particles on an individual site of the superlattice. The concentration is highest in the points of intersection. Sites of the superlattice with less than five particles on them have been left out for easier recognition.

A similar configuration was found by Tavazza, Landau and Adler [38]. The subject of their paper is a Si-Ge alloy with a compressible Ising model and Stillinger-Weber interaction.

This configuration was then used as initial configuration for a simulation at $T = 0$ without the constraint of the superlattice. The resulting configuration is shown in Fig. 3.15. While the

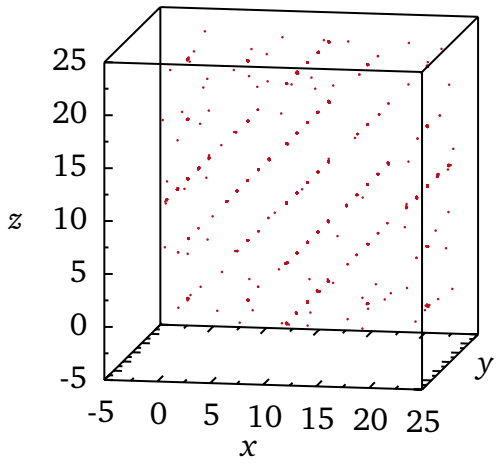

(a) Configuration in $d = 3$.

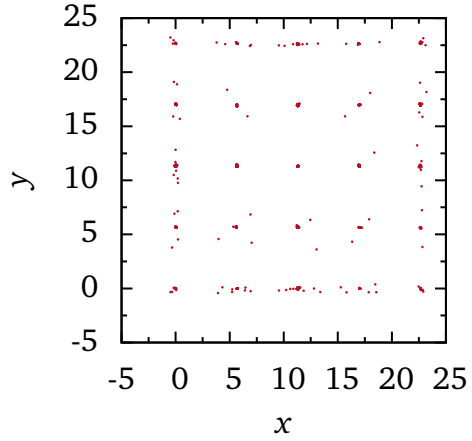

(b) Projection of the configuration onto the x-y plane.

Figure 3.15: Configuration for $L = 40$ and $T = 0$.

overall triple plane structure is preserved, the individual clusters are slightly bloated and there are some particles in the gaps as well. The distribution of bond lengths has two sharp peaks at $r \approx 0$ (at least $r \lesssim 10^{-4}$) and $r \approx 5.6$ (Fig. 3.16), similar to the one-dimensional ground state.

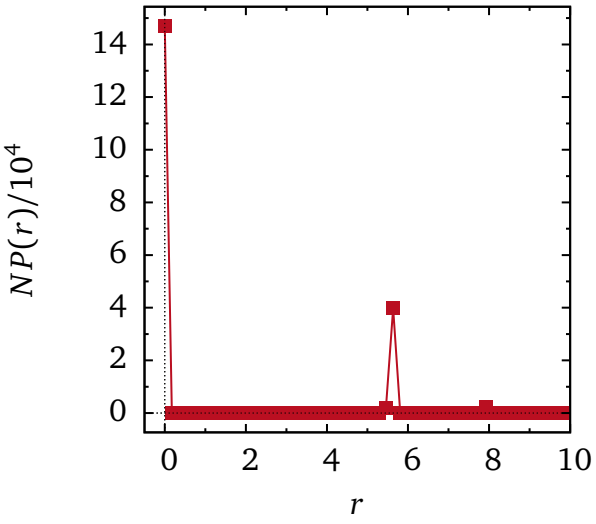

Figure 3.16: Distance histogram $P(r)$ for $L = 40$ and $T = 0$.

3.4 Magnetic Properties for $T > 0$

While for $T = 0$ all spins are equal, and therefore $m = 1$ constant, it remains to examine the effect of the clustering on the magnetic properties of the system at $T > 0$. For this purpose, several different temperatures have been simulated (Tab. 3.5). Simulation time can be kept rel-

L	T	κ	K	$t_{\max}/10^5$	δ
40	2	3	1	2	auto
40	8	3	1	2	auto
40	9	3	1	1	auto

Table 3.5: Simulation parameters.

atively short, since reasonable initial configurations are available and thermodynamic averages are not of interest. From each run, only the configuration of lowest energy is extracted.

$T = 2$

For $T = 2$, the triple-plane configuration is still clearly identifiable from Fig. 3.17. Most of the particles are located in three perpendicular planes, while the particles are densest in the points of intersection. The bond length is distributed in two sharp peaks with more weight at $r = 0$

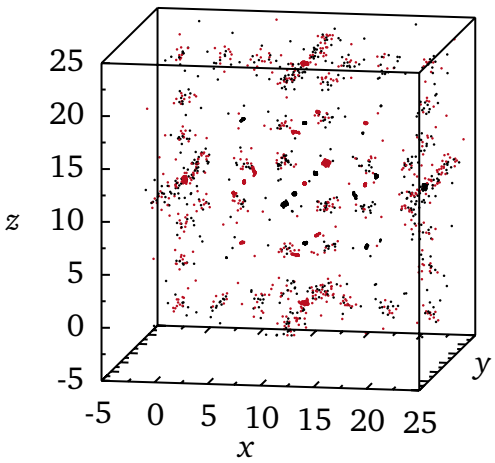

(a) Configuration in $d = 3$.

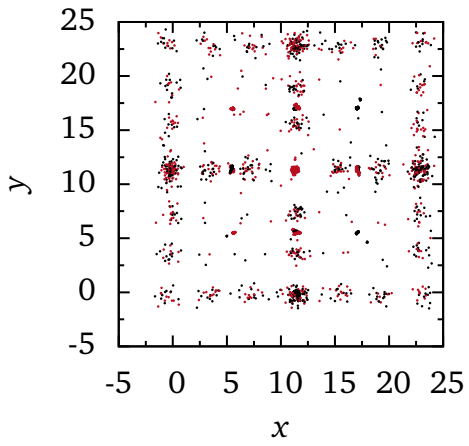

(b) Projection of the configuration into the x-y plane.

Figure 3.17: Configuration for $L = 40$ and $T = 2$. Colors indicate the orientation of the particle spin

(Fig. 3.18). This means, that the majority of particles is still located in $r \approx 0$ clusters. Within those clusters, all spins are equal, while separate clusters can have different magnetization. Whereas the correlation within the clusters is very strong, the correlation among individual clusters is very weak. This is due to the high value of κ. The magnetic part of the interaction

$$u_{\text{mag}}^{(ij)}(r) = -S_i S_j \exp\bigl(-\kappa(r_{ij} - 1)\bigr) \tag{3.28}$$

is independent of κ at $r = 1$. For large κ the interaction becomes rapidly stronger for $r < 1$ and decays fast for $r > 1$. As a consequence, we have magnetic order on a microscopic scale, where $r < 1$, and magnetic order on a macroscopic scale, where $r > 1$.

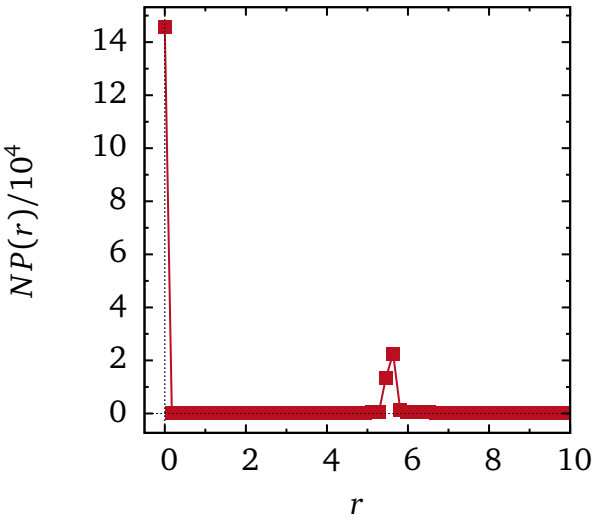

Figure 3.18: Distance histogram $P(r)$ for $L = 40$ and $T = 2$.

Because the clusters can only change magnetization as a whole, the magnetization becomes discretized to some degree. This becomes apparent when looking at Fig. 3.19. In the time series as well as in the histogram there are 'forbidden' values of the magnetization which are never assumed. The explanation for this is straightforward: If a system consists of n clusters, each having either $m_i = -1$ or $m_i = 1$, $i = 1 \ldots n$, then there are only $n + 1$ different values of the magnetization[3].

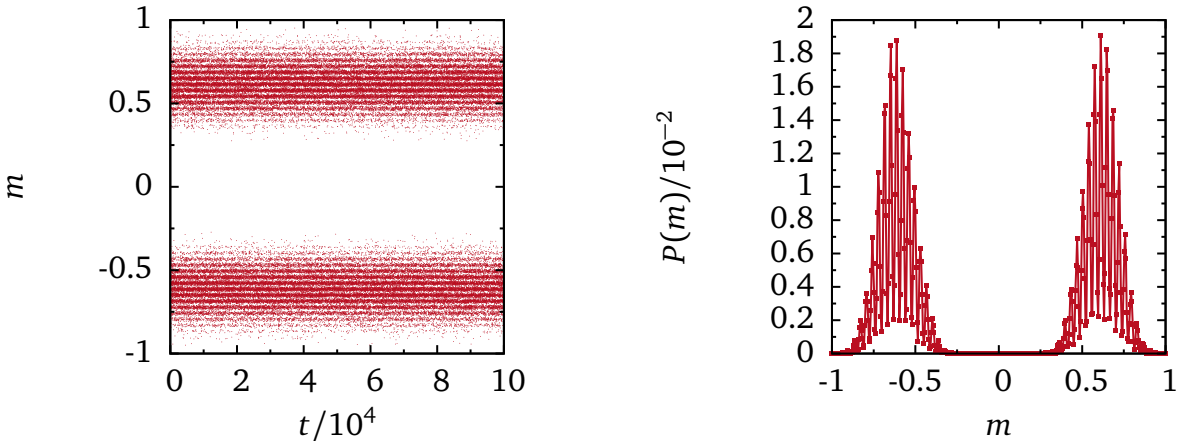

(a) Time series of the magnetization $m(t)$.

(b) Histogram of the magnetization $P(m)$.

Figure 3.19: Magnetic properties of the system for $L = 40$ and $T = 2$.

$T = 8$

When looking at the configuration for $T = 8$, the triple-plane structure is still visible in Fig. 3.20. The right peak of the bond-length distribution in Fig. 3.24 is broadened as opposed to the left peak, which is still very narrow. This means, that there still are compact

[3] The same actually holds for unclustered systems, because of the finite number of spins. This becomes especially important for small systems and has to be considered when computing the histogram.

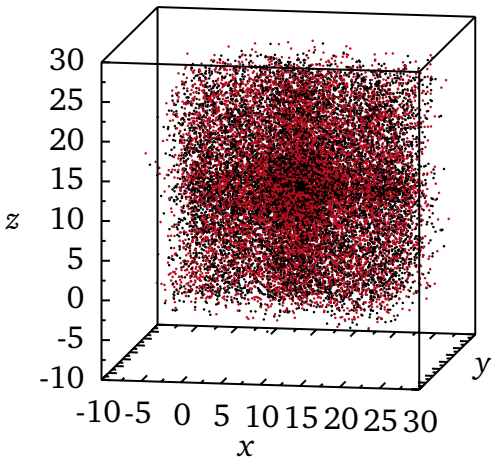

(a) Configuration in $d = 3$.

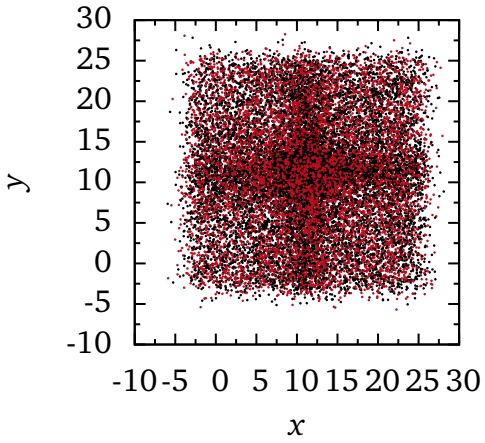

(b) Projection of the configuration into the x-y plane.

Figure 3.20: Configuration for $L = 48$ and $T = 8$.

clusters in the system. A discretization of magnetization is not visible anymore with the current

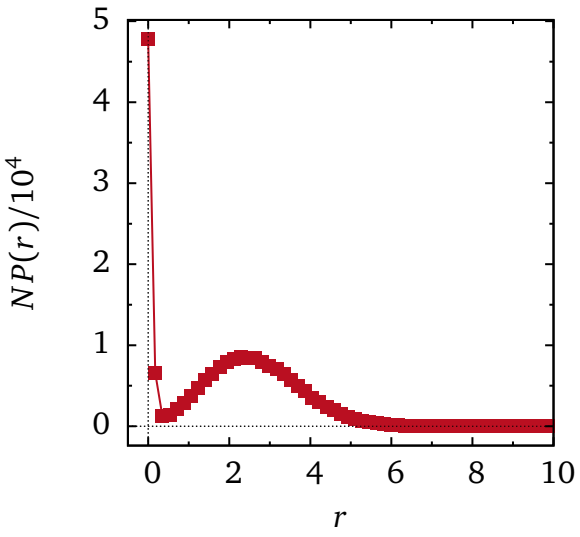

Figure 3.21: Distance histogram $P(r)$ for $L = 40$ and $T = 8$.

resolution. However, there are two distinct peaks in the histogram Fig. 3.22b, indicating, that the macroscopic system is still in the magnetically ordered phase at this temperature.

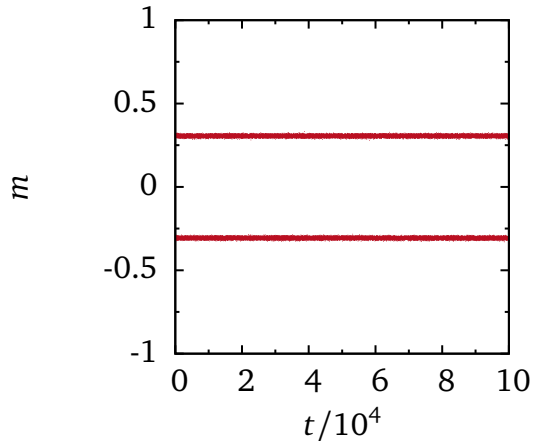

(a) Time series of the magnetization $m(t)$.

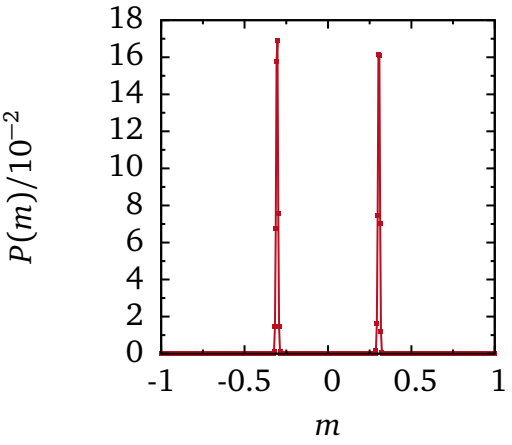

(b) Histogram of the magnetization $P(m)$.

Figure 3.22: Magnetic properties of the system for $L = 40$ and $T = 8$.

$T = 9$

From $T = 8$ to $T = 9$, the characteristics of system undergo some severe changes. Firstly,

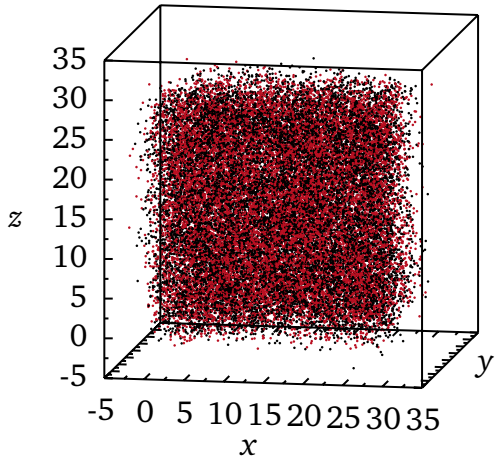

(a) Configuration in $d = 3$.

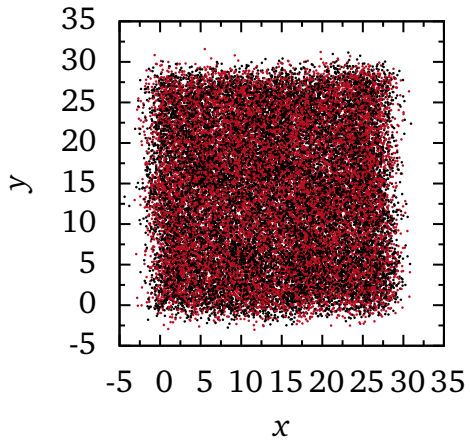

(b) Projection of the configuration into the x-y plane.

Figure 3.23: Configuration for $L = 40$ and $T = 9$.

the bond length distribution Fig. 3.24 has now only one peak at $r > 0$ and no peak at $r = 0$ meaning that there are no more $r = 0$ clusters forming. Also the triple-plane structure is not visible anymore in Fig. 3.23. This can be seen as a fundamental transition in configuration. Secondly, the histogram of the magnetization Fig. 3.25 has now only one peak at $m = 0$; the system is now in the magnetically disordered phase. Hence, between $T = 8$ and $T = 9$, there are not one but *two fundamental transitions*. It remains to identify, whether those transitions share a critical temperature or whether they occur separately.

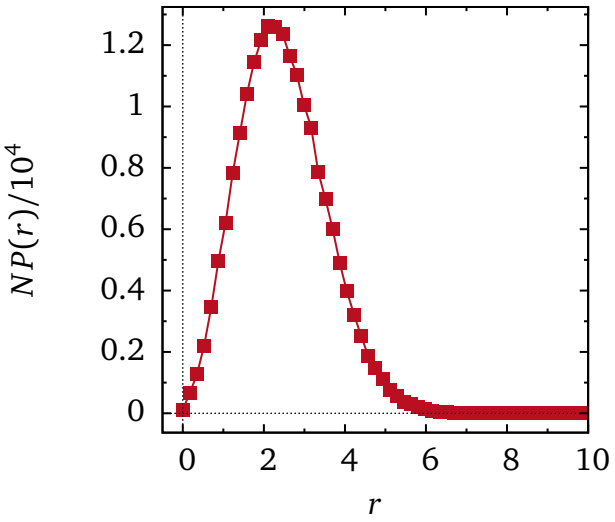

Figure 3.24: Distance histogram $P(r)$ for $L = 40$ and $T = 9$.

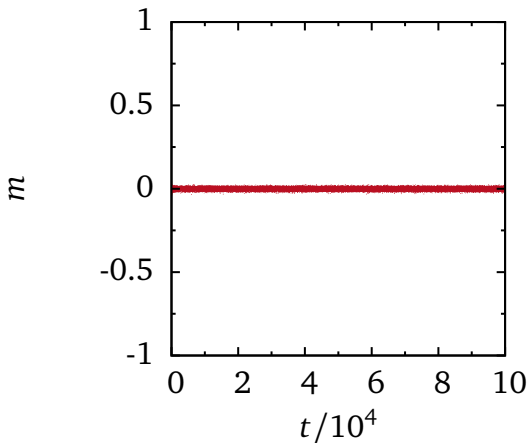

(a) Time series of the magnetization $m(t)$.

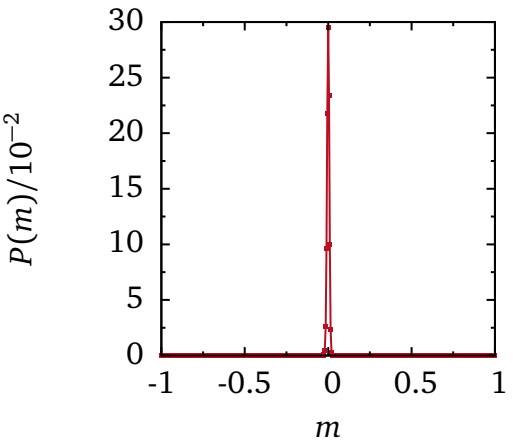

(b) Histogram of the magnetization $P(m)$.

Figure 3.25: Magnetic properties of the system for $L = 40$ and $T = 9$.

3.5 Summary

In Chapter 2, a field theory for the Ising model with coupling to elastic degrees of freedom was derived. During the derivation, a linear theory of elasticity was assumed. This allows for the microscopic elastic fluctuations to be integrated out. Further analysis of the effective Hamiltonian showed, that the system should at constant volume exhibit Fisher renormalized exponents.

The evaluation in Section 3.2 revealed, that the exponents can by no means considered to be Fisher renormalized, but instead are closer to those of the regular Ising model. One possible explanation for this behavior is the choice of parameters. A glance at the distribution of the coupling parameter $P(J)$ showed, that the width of the distribution is small compared to $k_\mathrm{B}T$. This is an indication, that the coupling might be too weak for the given parameters. The width of $P(J)$ can be increased significantly by decreasing the constant of elastic interaction K and increasing the constant of magnetic decay κ.

In Section 3.3 this new set of parameters was examined at $T = 0$. Since the convergence to the ground state is rather poor, even with simulated annealing methods, the one-dimensional case was examined first. It was found, that the particles arrange in multiple equidistant clusters, where within one cluster the particle distance is close to zero, if not zero. This is because on the one hand the particles want to minimize interparticle distance, and on the other hand avoid overly stretched bonds due to the periodic boundary conditions. It was found, that there is an optimal cluster distance, that is independent of system size.

This observation was then transferred to the three-dimensional case. In a first step, the particles were confined to a superlattice, and therefore forced to assume a clustered configuration. This way the configuration space was reduced and the convergence to the ground state improved. It was found, that the particle arrange in three mutually perpendicular planes. Similarly to the one-dimensional case, interparticle distance was minimized, while not allowing for excessively stretched bonds.

This configuration was then used as a starting point for a simulation without the restriction of the superlattice. Indeed the clustered triple-plane configuration remained intact, even without the constraint.

As the system is heated up, the magnetization is allowed to fluctuate again and some interesting behavior arises. Within a cluster the magnetic interaction is so strong, that the magnetization of a single cluster is essentially unity. The correlation between individual clusters on the other hand is weak enough, that it allows for different magnetization among individual clusters. There is a superposition of order on the microscopic scale and disorder on the macroscopic scale.

As the system is heated up further, the clustering dissolves. This means, that additional to the magnetic transition, there is a second, structural transition. Within the limits of this work, it could not yet be verified, whether or not this transition occurs at the same temperature as the first one.

3.6 Conclusion and Outlook

In Chapter 2 it was derived, that the phase transition at constant volume should be of second order with Fisher renormalized exponents. This however is based on the assumption of linear elasticity, which allows for the elimination of the microscopic elastic fluctuations from the effective Hamiltonian.

In the evaluation, those Fisher renormalized exponents could not be confirmed. The found exponents are in fact closer to the regular Ising exponents. Since all elastic fluctuations where included in the simulation, this might be an indication that the assumption of linear elasticity is invalid.

In order to collect further evidence, one could consider checking the predictions for the constant pressure case as well. However, since the transition in this case is expected to be of weak first order [39], this might prove to be rather challenging.

Another possible explanation is, that the effects of elastic coupling are just too weak for the first set of parameters. Because of this, a second set of parameters was proposed in order to soften the lattice and to accelerate the decay of magnetic interaction. When examining the ground state it was found, that the particles tend to form compact clusters, where within a cluster the bond length of neighboring particles is close to zero if not zero.

In addition to the magnetic phase transition, there is a transition from a clustered to an unclustered state as temperature is raised. It is not yet clear, whether both transitions occur at the same temperature, nor is it clear, whether the structural transition can be considered first or second order.

Also, it still has to be examined, if the magnetic transition still is of second order and if the values of the critical exponents change in comparison with the first parameter set.

In real solids there usually are strong repulsive interactions for very short distances, that would prevent an overly compact clustering. Such a repulsion could be added to the model by including a term $\propto r^{-b},\ b > d$ in the potential.

Clearly, the physics of the given model is more complex than it was assumed at the beginning of the project.

List of Figures

List of Tables

References

[1] B. Dünweg and D. P. Landau, "Phase diagram and critical behavior of the Si-Ge unmixing transition: A Monte Carlo study of a model with elastic degrees of freedom," *Physical Review B*, vol. 48, pp. 14182–14197, Nov. 1993.

[2] G. Tkacik, E. Schneidman, M. J. Berry II, and W. Bialek, "Ising models for networks of real neurons," *arXiv:q-bio/0611072*, Nov. 2006. arXiv: q-bio/0611072.

[3] M. E. Fisher, "Renormalization of Critical Exponents by Hidden Variables," *Physical Review*, vol. 176, pp. 257–272, Dec. 1968.

[4] B. Dünweg, "Computersimulationen zu Phasenübergängen und kritischen Phänomenen," 2000.

[5] G. A. Baker and J. W. Essam, "Effects of Lattice Compressibility on Critical Behavior," *Physical Review Letters*, vol. 24, pp. 447–449, Mar. 1970.

[6] F. J. Wegner, "Magnetic phase transitions on elastic isotropic lattices," *Journal of Physics C: Solid State Physics*, vol. 7, no. 12, p. 2109, 1974.

[7] J. Sak, "Critical behavior of compressible magnets," *Physical Review B*, vol. 10, pp. 3957–3960, Nov. 1974.

[8] D. J. Bergman and B. I. Halperin, "Critical behavior of an Ising model on a cubic compressible lattice," *Physical Review B*, vol. 13, no. 5, pp. 2145–2175, 1976.

[9] A. Tröster, "Evidence for Fisher Renormalization in the Compressible ϕ^4 Model," *Physical Review Letters*, vol. 100, p. 140602, Apr. 2008.

[10] L. D. Landau and E. M. Lifshitz, *Statistical Physics*, vol. 5. Elsevier, 3 ed., 2012.

[11] P. M. Chaikin and T. C. Lubensky, *Principles of Condensed Matter Physics*. Cambridge ; New York, NY, USA: Cambridge University Press, annotated edition ed., June 1995.

[12] L. D. Landau, "On the theory of phase transitions. I.," *Zh. Eksp. Teor. Fiz.*, vol. 11, p. 19, 1937.

[13] L. D. Landau, L. P. Pitaevskii, A. M. Kosevich, and E. M. Lifshitz, *Theory of Elasticity, Third Edition: Volume 7*. Amsterdam: Butterworth-Heinemann, 3 edition ed., Jan. 1986.

[14] B. Dünweg, "Simulation of phase transitions: critical phenomena," in *Monte Carlo and Molecular Dynamics of Condensed Matter Systems* (K. Binder and Ciccotti, eds.), vol. 49 of *Conference Proceedings*, Bologna: SIF, 1996.

[15] K. Binder and D. P. Landau, "Finite-size scaling at first-order phase transitions," *Physical Review B*, vol. 30, pp. 1477–1485, Aug. 1984.

[16] A. M. Ferrenberg and R. H. Swendsen, "New Monte Carlo technique for studying phase transitions," *Physical Review Letters*, vol. 61, pp. 2635–2638, Dec. 1988.

[17] A. M. Ferrenberg and R. H. Swendsen, "Optimized Monte Carlo data analysis," *Physical Review Letters*, vol. 63, pp. 1195–1198, Sept. 1989.

[18] H. Flyvbjerg and H. G. Petersen, "Error estimates on averages of correlated data," *The Journal of Chemical Physics*, vol. 91, pp. 461–466, July 1989.

[19] P. C. Hohenberg and B. I. Halperin, "Theory of dynamic critical phenomena," *Reviews of Modern Physics*, vol. 49, pp. 435–479, July 1977.

[20] R. H. Swendsen and J.-S. Wang, "Nonuniversal critical dynamics in Monte Carlo simulations," *Physical Review Letters*, vol. 58, pp. 86–88, Jan. 1987.

[21] J.-S. Wang and R. H. Swendsen, "Cluster Monte Carlo algorithms," *Physica A: Statistical Mechanics and its Applications*, vol. 167, pp. 565–579, Sept. 1990.

[22] J. Du, B. Zheng, and J.-S. Wang, "Dynamic critical exponents of Swendsen-Wang and Wolff algorithms by nonequilibrium relaxation," *Journal of Statistical Mechanics: Theory and Experiment*, vol. 2006, pp. P05004–P05004, May 2006. arXiv: cond-mat/0603038.

[23] J. Hoshen and R. Kopelman, "Percolation and cluster distribution. I. Cluster multiple labeling technique and critical concentration algorithm," *Physical Review B*, vol. 14, pp. 3438–3445, Oct. 1976.

[24] M. D. D. Meo, D. W. Heermann, and K. Binder, "Monte Carlo study of the ising model phase transition in terms of the percolation transition of "physical clusters"," *Journal of Statistical Physics*, vol. 60, pp. 585–618, Sept. 1990.

[25] J. C. Maxwell, "L. on the calculation of the equilibrium and stiffness of frames," *The London, Edinburgh, and Dublin Philosophical Magazine and Journal of Science*, vol. 27, no. 182, pp. 294–299, 1864.

[26] D. Frenkel and B. Smit, *Understanding Molecular Simulation: From Algorithms to Applications*. San Diego: Academic Press, 2nd revised edition. ed., 2001.

[27] A. Tröster and C. Dellago, "The Fourier Monte Carlo Approach to Lattice Spin Models," *Physics Procedia*, vol. 6, pp. 106–116, 2010.

[28] A. Tröster, "High Precision Fourier Monte Carlo Simulation of Crystalline Membranes," *Physical Review B*, vol. 87, Mar. 2013. arXiv: 1303.3726.

[29] R. P. Fedorenko, "The speed of convergence of one iterative process," *USSR Computational Mathematics and Mathematical Physics*, vol. 4, no. 3, pp. 227–235, 1964.

[30] A. Sokal, "Monte Carlo Methods in Statistical Mechanics: Foundations and New Algorithms," in *Functional Integration* (C. DeWitt-Morette, P. Cartier, and A. Folacci, eds.), no. 361 in NATO ASI Series, pp. 131–192, Springer US, 1997. DOI: 10.1007/978-1-4899-0319-8_6.

[31] A. M. Ferrenberg and D. P. Landau, "Critical behavior of the three-dimensional Ising model: A high-resolution Monte Carlo study," *Physical Review B*, vol. 44, pp. 5081–5091, Sept. 1991.

[32] K. Binder, “Finite size scaling analysis of ising model block distribution functions,” *Zeitschrift für Physik B Condensed Matter*, vol. 43, pp. 119–140, June 1981.

[33] J. C. Le Guillou and J. Zinn-Justin, “Critical Exponents for the n-Vector Model in Three Dimensions from Field Theory,” *Physical Review Letters*, vol. 39, pp. 95–98, July 1977.

[34] S. Kirkpatrick, C. D. Gelatt, and M. P. Vecchi, “Optimization by Simulated Annealing,” *Science*, vol. 220, pp. 671–680, May 1983.

[35] V. Černý, “Thermodynamical approach to the traveling salesman problem: An efficient simulation algorithm,” *Journal of Optimization Theory and Applications*, vol. 45, pp. 41–51, Jan. 1985.

[36] C.-R. Hwang, “Simulated annealing: Theory and applications,” *Acta Applicandae Mathematica*, vol. 12, pp. 108–111, May 1988.

[37] M. A. R. Strobl and D. Barker, “On simulated annealing phase transitions in phylogeny reconstruction,” *Molecular Phylogenetics and Evolution*, vol. 101, pp. 46–55, Aug. 2016.

[38] F. Tavazza, D. P. Landau, and J. Adler, “Phase diagram and structural properties for a compressible Ising ferromagnet at constant volume,” *Physical Review B*, vol. 70, p. 184103, Nov. 2004.

[39] A. I. Larkin and S. A. Pikin, “Phase Transitions of the First Order but Nearly of the Second,” no. 29, p. 891, 1969.

Index